

Article

Impact of Spotted Hyena Optimized Cascade Controller in Load Frequency Control of Wave-Solar-Double Compensated Capacitive Energy Storage Based Interconnected Power System

Arindita Saha ¹, Puja Dash ² , Naladi Ram Babu ³ , Tirumalasetty Chiranjeevi ^{4,*}, Bathina Venkateswararao ⁵ and Łukasz Knypinski ^{6,*} 

¹ Department of Electrical Engineering, Regent Education & Research Foundation Group of Institutions, Kolkata 700121, West Bengal, India

² Department of Electrical and Electronics Engineering, Gayatri Vidya Parishad College of Engineering (Autonomous), Visakhapatnam 530048, Andhra Pradesh, India

³ Department of Electrical & Electronics Engineering, Aditya Engineering College, Surampalem 533437, Andhra Pradesh, India

⁴ Department of Electrical Engineering, Rajkiya Engineering College Sonbhadra, Sonbhadra 231206, Uttar Pradesh, India

⁵ Department of EEE, V R Siddhartha Engineering College, Vijayawada 520007, Andhra Pradesh, India

⁶ Institute of Electrical Engineering and Electronics, Faculty of Automatic Control, Robotic and Electrical Engineering, Poznan University of Technology, 60-965 Poznan, Poland

* Correspondence: chirupci479@gmail.com (T.C.); lukasz.knypinski@put.poznan.pl (Ł.K.)



Citation: Saha, A.; Dash, P.; Babu, N.R.; Chiranjeevi, T.; Venkateswararao, B.; Knypinski, Ł. Impact of Spotted Hyena Optimized Cascade Controller in Load Frequency Control of Wave-Solar-Double Compensated Capacitive Energy Storage Based Interconnected Power System. *Energies* **2022**, *15*, 6959. <https://doi.org/10.3390/en15196959>

Academic Editor: Juri Belikov

Received: 22 August 2022

Accepted: 15 September 2022

Published: 22 September 2022

Publisher's Note: MDPI stays neutral with regard to jurisdictional claims in published maps and institutional affiliations.



Copyright: © 2022 by the authors. Licensee MDPI, Basel, Switzerland. This article is an open access article distributed under the terms and conditions of the Creative Commons Attribution (CC BY) license (<https://creativecommons.org/licenses/by/4.0/>).

Abstract: The concept of automatic generation control has an immense role in providing quality power in an interconnected system. To obtain quality power by controlling the oscillations of frequency and tie-line power, a proper controller design is necessary. So, an innovative endeavor has been undertaken to enforce a two-stage controller with the amalgamation of a proportional-derivative with filter (PDN) (integer-order) and a fractional order integral-derivative (FOID), i.e., PDN(FOID). In an effort to acquire the controller's gains and parameters, a bio-inspired meta-heuristic spotted hyena optimizer is applied. Various examinations manifest the excellence of PDN(FOID) over other controllers such as integral, proportional-integral, proportional-integral-derivative filter, and fractional order PID from perspectives concerning the diminished amount of peak anomaly oscillations, and the instant of settling for a three-area system. The system includes thermal-bio-diesel in area-1; a thermal-geothermal power plant in area-2; and a thermal-split-shaft gas turbine in area-3. It is also observed that the presence of renewable sources such as wave power plants and photovoltaics makes the system significantly better compared to the base system, when assessed individually or both together. Action in a combination of capacitive energy storage with duple compensation is also examined using the PDN(FOID) controller, which provides a noteworthy outcome in dynamic performance. Moreover, PDN(FOID) parameter values at a nominal condition are appropriate for the random patterns of disturbance needed for optimization.

Keywords: Archimedes wave energy conversion; automatic generation control; bio-diesel plant; capacitive energy storage; geothermal power plant; PDN(FOID) controller; PV; spotted hyena optimizer; wave power plant

1. Introduction

The principle of automatic generation control (AGC) is to maintain the balance between power generation and power demand along with losses [1–3]. If this equilibrium is not maintained then it will lead to excessive fluctuations from the nominal values of frequency and tie-line power connecting areas. Back in earlier days, most of the literature in AGC learning highlighted work in isolated systems [4–6]. Later works were reported on interconnected systems for two-area, and even five-area, thermal systems [7–12]. Nowadays,

the literature reflects the usage of multiple sources as generating units such as hydro, gas, and diesel along with thermal as a base generating unit [13–16]. However, far fewer works have been reported on another form of gas turbine, which is the split-shaft gas turbine (Ss (GT)) [17]. So, many studies can be conducted on thermal-Ss (GT) systems.

The increasing use of the same conventional sources is extensively depleting them. Conventional sources also affect the environment with their many by-products, which calls for the association of renewable sources with conventional means. The most common forms of renewable sources that are readily available are solar and wind. Many works have been reported in the literature about the involvement of solar and wind in AGC learning in a single area as well as in interconnected systems. Arya [18] reported on the use of a photovoltaic (PV) system in a hydro-thermal system. In addition to these, geothermal and bio-diesel are also coming into the picture. Geothermal energy is a type of thermal energy that is stored by the earth itself. Thus, this type of energy can be extracted from the earth's crust. Tasnin et al. [19] reported on the application of geothermal in AGC learning. Bio-diesel plants utilize bio-diesel to drive generators. Bio-diesel is produced from oil that has been extracted from various plants such as sunflower, palm, or soybean. The most common form is the use of palm oil. Bio-diesel is a type of renewable fuel. Barik et al. [20] highlighted the use of bio-diesel in an isolated system. In addition, wave power plants (WavePPts) have found minimal consideration in AGC. WavePPts have Archimedes energy translation parts that convert wave energy into electrical energy. Hasanien et al. [21] united a WavePPt with AGC knowledge for a dual-arena thermal scheme. The amalgamation of a geothermal power plant (GPP) and a bio-diesel plant along with a WavePPt and photovoltaic (PV) in AGC learning has not yet been reflected in the literature. Thus, a thermal-Ss (GT) system incorporating GPP, bio-diesel, a WavePPt, and PV calls for further extensive assessments.

The perception of AGC leads to a great effort to decrease the anomaly of frequency along with tie-line power, interlinking diverse areas from their basic value. However, periodically, a state may ascend when oscillations grow to an excessive amount so that a scheme might bring uncertainty. In this circumstance, if the scheme is involved with an energy storage unit, such as capacitive energy storage (C^{ES}), then it can avoid such an alteration. As such, C^{ES} will draw an extra amount of power, which indicates less usage of kinetic energy to subdue small load needs. C^{ES} [22] has found its application in AGC learning. It can be used in the existence of duple compensation or in the absence. The influence of the contrast of C^{ES} with/without duple compensation on scheme dynamics is hitherto to be discovered.

In the scheme of AGC knowledge, there is a dual diverse sort of control similar to a primary control and subordinate control. A major consideration in AGC knowledge concerning control is the appropriate choice of secondary controllers. Numerous categories of subordinate controllers such as integer order (InO), fractional order (FrO), and cascade controllers are described in the literature associated with AGC. Diverse authors have described numerous InO controllers, such as integral (I) [23], proportional–integral (PI) [24], and proportional–integral–derivative with filter (PIDN) [25], in AGC. Dual [26] or trio [27] higher grade of freedom subordinate controllers have also been examined in this arena of learning, and correspond to the InO sort. The few FrO controllers, which initiate its application, are FOPI [28] and FOPIDN [29]. The AGC knowledge literature reflects the practice of InO order two-stage controllers PD-PID [30], and FrO two-stage controllers FOPI-FOPD [19], as well as a grouping of InO and FrO controllers (PIDN-FOPD) [31]. A dual-stage controller with the amalgamation of InO PDN with FrO FOID, termed PDN(FOID), is never hitherto specified in AGC works. Furthermore, the utilization of the PDN(FOID) subordinate controller in this trio-area thermal–bio-diesel–GPP-Ss (GT) scheme along with WavePPt, PV, and CES has not been stated beforehand, so it claims the necessity of examination.

The performance of each subservient controller is exceptionally solitary if the finest amount of gain and related constraints are appropriately favored. These could be executed with the assistance of typical or optimization measures. However, the usage of typical

methods such as straight pursuit, arbitrary pursuit, incline pursuit, and numerous others is pretty arduous and delivers substandard consequences, as well as craving a great number of repetitions to deliver outcomes. The optimization procedures that have previously been found in AGC knowledge are whale optimization algorithm (WOA) [17], bacterial foraging optimization (BFO) [24], cuckoo search (CS) [26], differential evolution (DE) [32], particle swarm optimization (PSO) [33], firefly algorithm (FA) [34], grey wolf optimization (GWO) [35], imperialist competitive algorithm (ICA) [36], flower pollination algorithm (FPA) [37], honey badger algorithm [38], AdaBoost algorithm [39], and improved moth-flame algorithm [40]. A newly developed bio-inspired meta-heuristic algorithm titled spotted hyena optimizer (SHO) [41] is obtainable from the literature. SHO was established from the behavioral nature of spotted hyenas, which portrays the social bond between the spotted hyena and their collaborative deeds. To our great surprise, the implementation of SHO has not been identified in AGC learning for its ability to obtain the best values of controller gains and parameters, and this demands a complete investigation.

With reference to the above-mentioned discussions, the prime purpose of the present article is as follows:

- Formulation of a three-area scheme with a thermal–bio–diesel in area-1, thermal–GPP in area-2, and thermal–Ss (GT) in area-3;
- The gains of I/PI/PIDN/PDN(FOID) are simultaneously optimized individually using the SHO algorithm in order to obtain an excellent controller;
- The scheme stated in (a) is combined with WavePPt in area-1, and its impact on the system dynamics is assessed;
- The scheme stated in (a) is combined with PV in area-3, and its impact on the system dynamics is assessed;
- The scheme stated in (a) is combined with WavePPt in area-1 and PV in area-3 together, and their impact on the system dynamics is assessed;
- The scheme stated in (e) is combined with C^{ES} with/without duple compensation separately, and their impact on the system dynamics is studied on an individual basis;
- Sensitivity investigation is undertaken to examine the toughness of the superlative ‘controller’s gains when subjected to a random pattern of load disturbance.

For ease of understanding, the present article is schematically represented in Figure 1.

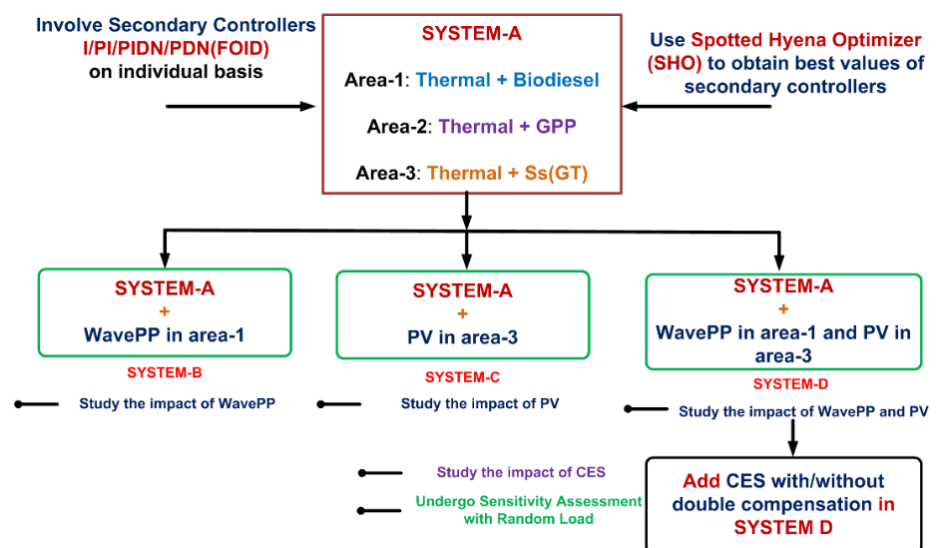


Figure 1. Schematic representation of the entire work.

2. Structure Portrayal

2.1. Overall Portrayal of Structure

A trio-area scheme of uneven sort is contemplated for scrutiny, confining the area size ratio in the arrangement of 2:3:4. The scheme encompasses a bio-diesel-thermal plant in area-1. In the same manner, thermal-geothermal power plants (GPP) in area-2, and thermal-split-shaft gas turbine (Ss (GT)) in area-3. The parameters values are provided in Appendix A. Typical diesel plants are currently being substituted by bio-diesel plants since they are nonpoisonous, as well being ecologically friendly, and pretty bulky with curtailed viscosity; additionally, they emit a relatively small amount of carbon monoxide. Thus, they could be employed as a reserve for power origination. The following comprises the valve controller and ignition engine. The first order transfer functions (Tfn) of the valve controller and ignition engine of a bio-diesel plant are detailed by (1) and (2) on an individual basis.

$$Tf_{valve\ regulator}^{Bio-diesel} = \frac{K^{VR}}{1 + sT^{VR}} \quad (1)$$

K^{VR} and T^{VR} are the bio-diesel plant valve regulator's gain and time constants individually.

$$Tf_{Combustion\ engine}^{Bio-diesel} = \frac{K^{CE}}{1 + sT^{CE}} \quad (2)$$

K^{CE} and T^{CE} are the bio-diesel plant combustion engine's gain and time constants individually.

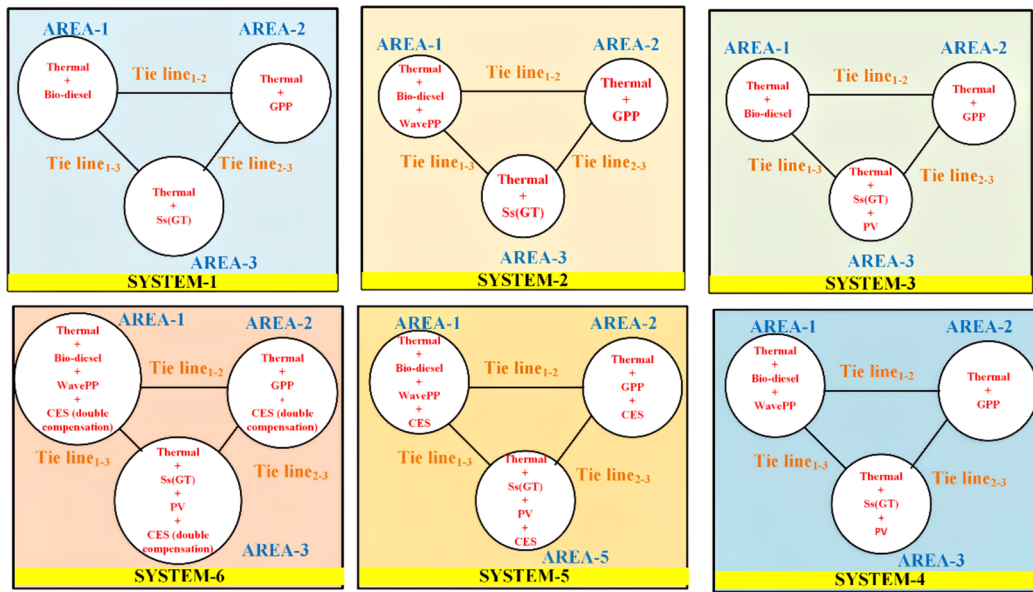
Geothermal energy is a potential renewable source (RWS) of energy where underground thermal energy is transformed into electricity. The Tfn modeling of GPP is similar to thermal plants, but it does not have a boiler for reheating steam [19]. The first order Tfn of the governor and turbine of GPP is given by (3) and (4), respectively.

$$Tf_n^{G_{GPP}} = \frac{1}{1 + sG^{GPP}} \quad (3)$$

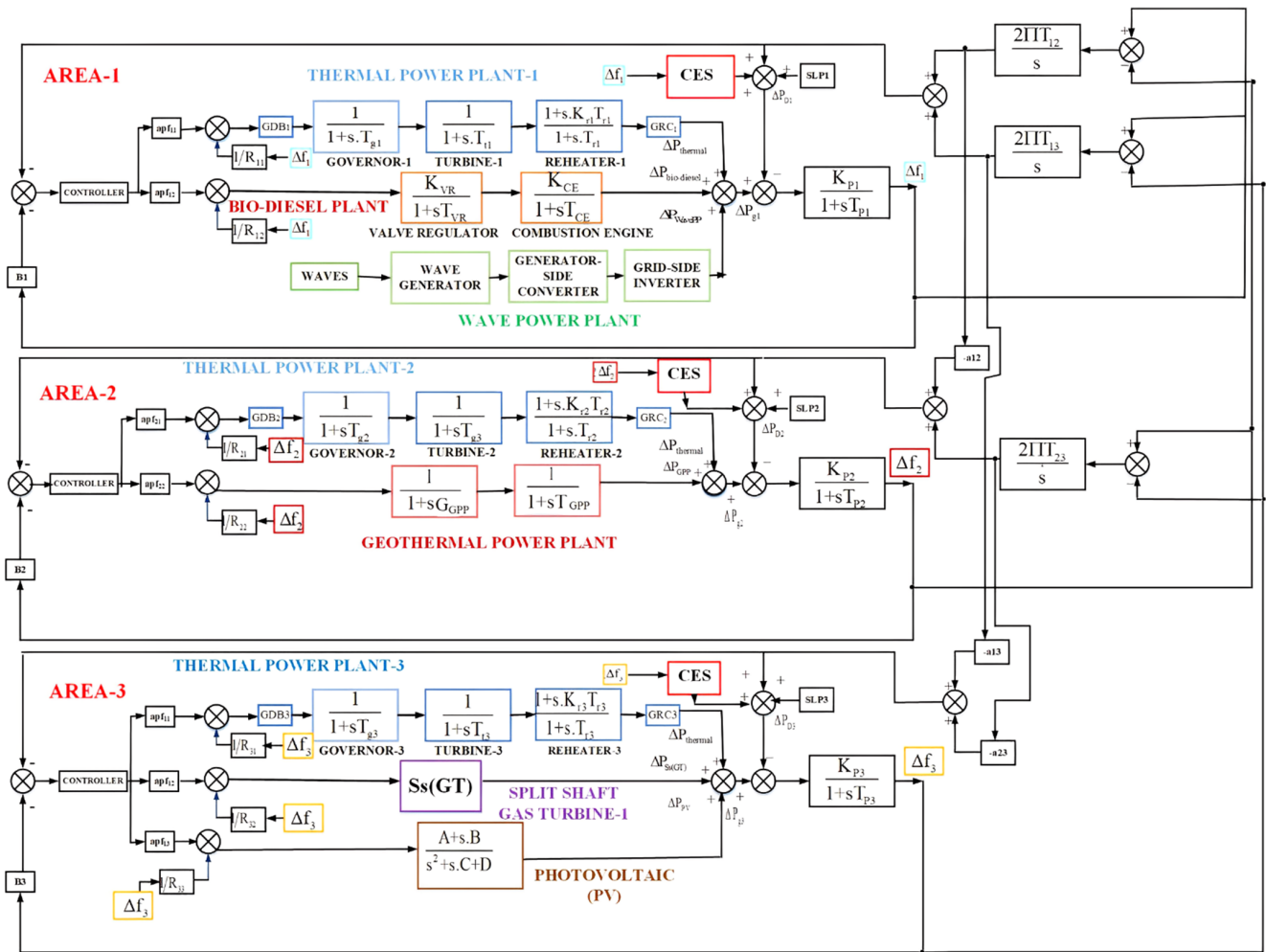
$$Tf_n^{T_{GPP}} = \frac{1}{1 + sT^{GPP}} \quad (4)$$

G^{GPP} and T^{GPP} are varied constants of GPP, independently. These values are obtained by the optimization technique SHO within the prescribed limits [19]. The participation factors (pf) of each generating unit of the respective areas are $pf_{11} = 0.7$, $pf_{12} = 0.3$ in area-1; $pf_{21} = 0.6$, $pf_{22} = 0.4$ in area-2; and $pf_{31} = 0.65$, $pf_{32} = 0.35$ in area-3. This is supposed to be scheme-1. Afterward, the structure is unified with a wave power plant (WavePPt) in area-1. This is supposed to be scheme-2. Afterward, structure-1 will be involved with the photovoltaic (PV) system in arena-3. This is scheme-3. Next, both the WavePPt and PV are integrated into scheme-1 with the WavePPt in area-1 and PV in area-3. This is scheme-4. When the WavePPt and PV are both present in the system, then the pf 's are: $pf_{11} = 0.7$, $pf_{12} = 0.3$ in arena-1; $pf_{21} = 0.6$, $pf_{22} = 0.4$ in arena-2; and $pf_{31} = 0.5$, $pf_{32} = 0.3$, and $pf_{33} = 0.2$ in arena-3. After that, the energy storing component, namely, capacitive energy storage (C^{ES}) is included in all areas. This is treated as scheme-5. Again, structure-5 is provided with C^{ES} having duple compensation in all areas. This is scheme-6. The representation and transfer function (Tfn) model of the arrangements is replicated in Figure 2. The Tfn model of Ss (GT) is obtained from [17]. The elementary values of structure parameters are specified in the addendum. The best values of controller gains and correlated constraints are attained with the assistance of the spotted hyena optimizer algorithm by taking into account the integral squared error as a performance index (Pi_{ISE}) specified by (5)

$$Pi_{ISE} = \int_0^T \{(\Delta f_1)^2 + (\Delta f_2)^2 + (\Delta f_3)^2 + (\Delta P_{tie_{1-2}})^2 + (\Delta P_{tie_{2-3}})^2 + (\Delta P_{tie_{1-3}})^2\} dt. \quad (5)$$



(a)



(b)

Figure 2. The representation and *Tfn* model of an unequal three-area system with thermal–biodiesel–WavePPt in area-1, thermal–GPP in area-2, and thermal–Ss (GT)–PV in area-3: (a) Schematic diagram of six different systems in a step-by-step method, (b) *Tfn* model of the ultimate system.

2.2. RWS—Wave Power Plant (WavePPt)

The power of the WavePPt is attained from sea surf. For accomplishing this rendition, Archimedes-wave swing (AdWS), which is a sort of translation segment pooled with a permanent magnet synchronous generator (PtMSg), converts sea surf mechanical to electrical energy. The Tf_n of AdWS attached to PtMSg is established. Here, the WavePPt is unified to area-1 through the assistance of a Converter | generator sideways/grid sideways inverter. All components of studied system were modelled MATLAB R2020a software. The converter present near a generator is employed in order to attain situations of extreme power point trailing. Mutually, the converter and inverter are intended for a gain value of 1 and a period constant of 0.01 s. The first order Tf_n prototype of AdWS of the WavePPt is specified by (6)

$$Tfn_{PPt_{AWS}^{Wave}} = \frac{K^{Wave}_{PPt_{AWS}}}{1 + sT^{Wave}_{PPt_{AWS}}}, \quad (6)$$

$K^{Wave}_{PPt_{AWS}}$ and $T^{Wave}_{PPt_{AWS}}$ are the gain and time constants of the AdWS of the WavePPt, respectively.

2.3. Energy Storage Device—Capacitive Energy Storage (C^{ES})

An energy storage device such as a capacitive energy storage device (C^{ES}) is equipment that usually employs a capacitor for storage along with a power adaptation segment, which is connected to the AC network with the assistance of a rectifier/inverter. The C^{ES} unit responds instantly to the system in the case of instant recurrent or current drift. Subsequently, any manner of unpredictability is moderated; C^{ES} yet again reestablishes the initial voltage amount in the plates of the capacitor by employing the additional energy obtainable in the scheme.

The Tfn of C^{ES} is specified by (7)

$$Tfn^{CES} = \frac{K^{CES}}{1 + sT^{CES}}, \quad (7)$$

K^{CES} is the gain and T^{CES} are the time constants of C^{ES} .

The C^{ES} plays the role of a frequency mediator in the case of a twofold compensation technique. The additive revision in power yield of C^{ES} with twofold compensation is detailed by (8)

$$\Delta P_{CES(duple\ compensation)} = \left[\frac{K^{CES(duple\ compensation)}}{1 + sT^{CES(duple\ compensation)}} \right] \left[\frac{1 + sT^1}{1 + sT^2} \right] \left[\frac{1 + sT^3}{1 + sT^4} \right] \Delta f_i(s), \quad (8)$$

$K^{CES(duple\ compensation)}$ and $T^{CES(duple\ compensation)}$ are the C^{ES} with duple compensation gain and time constants, individually. T^1 , T^2 , T^3 , and T^4 are varied time factors of the recompensed segment of C^{ES} .

3. The Proposed Approach

3.1. Problem Declaration

The emphasis of the present learning is on the frequency excursion approach with the utilization of an innovative metaheuristic method to optimize the InO and FrO amalgamated controller in a renewable source integrated power system structure. The main aim is to obtain a zero error for aberration in frequency and tie-line power by interconnecting different areas using a suitable control input.

3.2. Commended Controller

The commended controller is an aggregate of integer order (InO) together through a fractional order (FrO) controller. The commended controller is an I/O proportional-derivative with filter (PDN) with FrO integral-derivative (FOID), hence, PDN(FOID). The

arrangement of PDN(FOID) is substantiated in Figure 3. Segment-1 (B1) and Segment-2 (B2) are the layouts of PDN and FOID one-to-one. $Rs_i(s)$ is the antecedent signal and $Os_i(s)$ is the outcome signal for the PDN(FOID) controller. The *Trfn* of $B1_i(s)$ is manifested by (9)

$$B1_i(s) = \frac{K_{Pi}s + K_{Di}N_i}{(s + N_i)} \tag{9}$$

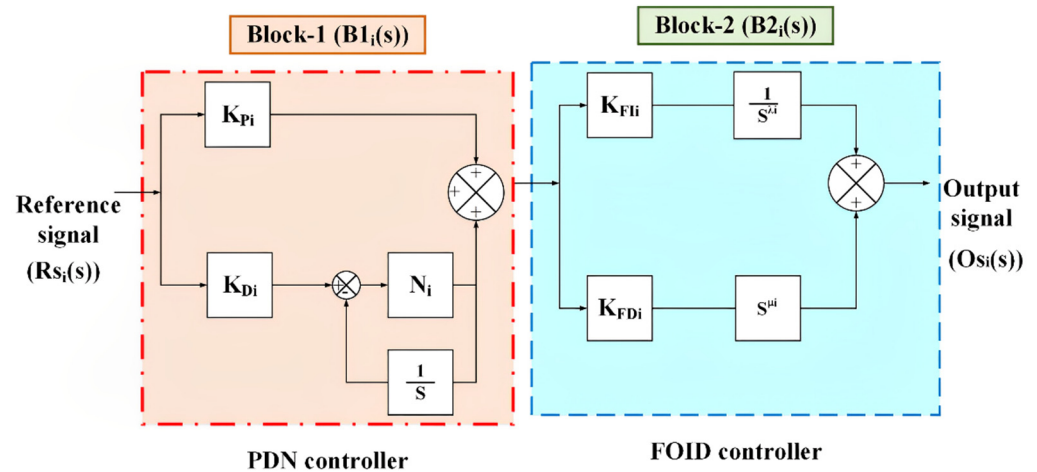


Figure 3. Layout of the proposed controller (PDN(FOID)).

The InO proportional gain is symbolized as K_{Pi} and the derivative gain as K_{Di} for the i -th suggested area, N_i is PDN controller’s filter. Summarization of Riemann–Liouville for the FrO integrator and derivative are obtainable from (10) and (11) [42–44]

$$\alpha D_t^{-\alpha} f(t) = \frac{1}{\Gamma(n)} \int_{\alpha}^t (t - \tau)^{\alpha-1} f(\tau) d\tau, \quad n-1 \leq \alpha < n, n \text{ is an integer} \tag{10}$$

$$\alpha D_t^{\alpha} f(t) = \frac{1}{\Gamma(n - \alpha)} \frac{d^n}{dt^n} \int_{\alpha}^t (t - \tau)^{n-\alpha-1} f(\tau) d\tau \tag{11}$$

αD_t^{α} is the fractional operator, and $\Gamma(\cdot)$ is the Euler’s gamma function. The alteration of the Fro integral and derivative in the Laplace domain is given by (12)

$$L\{\alpha D_t^{\alpha} f(t)\} = s^{\alpha} F(s) - \sum_{k=0}^{n-1} s^k \alpha D_t^{\alpha-k-1} f(t)|_{t=0} \tag{12}$$

The detriment of boundless computation of poles and zeros by virtue of absolute resemblance is manifested by Oustaloup, Mathieu, and Lanusse (1995) [45]. Here, a convenient Trfn is propounded that can approximate FrO derivatives together with integrators by dint of recursive distribution around poles and zeros substantiated by (13)

$$s^{\alpha} = K \prod_{n=1}^M \frac{1 + \left(\frac{s}{\omega_{Z,n}}\right)}{1 + \left(\frac{s}{\omega_{p,n}}\right)} \tag{13}$$

Suppose, attuned gain $K = 1$, gain = 0 dB through 1 rad/s frequency, $M =$ Count of poles along with zeros (fixed beforehand), and frequencies choice for poles and zeros are manifested by (14)–(18).

$$\omega_{Z,l} = \omega_l \sqrt{n} \tag{14}$$

$$\omega_{p,n} = \omega_{Z,n} \varepsilon, \quad n = 1, \dots, M \tag{15}$$

$$\omega_{Z,n+1} = \omega_{p,n} \sqrt{\eta} \quad (16)$$

$$\varepsilon = \left(\frac{\omega_h}{\omega_l} \right)^{\frac{v}{M}} \quad (17)$$

$$\eta = \left(\frac{\omega_n}{\omega_l} \right)^{\frac{(1-v)}{M}} \quad (18)$$

The Trfn of $B2_i(s)$ is manifested by (19).

$$B2_i(s) = \frac{K_{FIi}}{s^{\lambda_i}} + s^{\mu_i} K_{FDi} \quad (19)$$

In the above expressions, λ is the FrO integrator's fragment and μ is the FrO derivative's fragment. K_{FIi} is the FrO's integral fragment gain, and K_{FDi} is the FrO's derivative fragment gain of the suggested area.

3.3. Objective Function

The main purpose of the controller design is the proper optimization task including the minimization of a particular cost function considering the constraints of controller gains and parameters with its confines. Here, in the present AGC learning, an integral squared error (ISE) is involved as the cost function. The mathematical expression of ISE as a performance index is provided by (20).

$$Pi_{ISE} = \int_0^T \left\{ (\Delta f_i)^2 + (\Delta P_{tie_{i-j}})^2 \right\} dt. \quad (20)$$

Here, i and j are number of areas, where $i = 1, 2, 3$, and $i \neq j$.

In (20), the independent variables are K_P , K_D , N , K_{FI} , λ , K_{FD} , and μ , and the assumed constraints are provided in (21).

$$K_P^{min} \leq K_P \leq K_P^{max}, K_D^{min} \leq K_D \leq K_D^{max}, N^{min} \leq N \leq N^{max}, K_{FI}^{min} \leq K_{FI} \leq K_{FI}^{max}, \lambda^{min} \leq \lambda \leq \lambda^{max}, K_{FD}^{min} \leq K_{FD} \leq K_{FD}^{max}, \mu^{min} \leq \mu \leq \mu^{max} \quad (21)$$

4. Spotted Hyena Optimizer

Spotted Hyenas Optimizers (SHOs) are known as competent chasers. They are the bulkiest of the hyena breed. The spotted hyenas are also renowned as laughing hyenas since they sound like humans laughing. They are highly complex, brainy, and hugely communal creatures. The SHs trail their victims by their vision, auditory, and odor features. This nature of SH inspired Dhiman et al. [41] to develop the meta-heuristic algorithm SHO. The authors have outlined the mathematical design of the communal acquaintance of SH and collegial agility to undergo optimization. The trio events allied with SHO are tracking down capture, encompassing, and conspicuous capture.

1. Encompassing capture: To develop the numerical prototype, it is assumed that the present finest contender is the destined capture, which is closest to the optimum given that the chase arena was not known previously. The remaining chase agents will seek to renew their spot with reference to the response of the finest contender about the finest location. The numerical prototype is manifested by (22) and (23)

$$\vec{D}_h = \left| \vec{B} \cdot \vec{P}_p(x) - P(x) \right| \quad (22)$$

$$\vec{P}(x+1) = \vec{P}_p(x) - \vec{E} \cdot \vec{D}_h \quad (23)$$

In the above expressions, \vec{D}_h is the stretch between the Pr of the hunt, and \vec{P} is the spot vector of SH. \vec{B} and \vec{E} are computed as in (24)–(26)

$$\vec{B} = 2r\vec{d}_1 \quad (24)$$

$$\vec{B} = 2hr\vec{d}_2 - \vec{h} \quad (25)$$

$$\vec{h} = 5 - \left(\text{iteration} * \left(\frac{5}{\max_{\text{iteration}}} \right) \right), \text{ iteration} = 1, 2, 3 \dots, \max_{\text{iteration}} \quad (26)$$

For appropriately corresponding the exploration and exploitation, \vec{h} in straight line declined from 5 to 0 over the duration of the maximum iteration. Additionally, this execution indorses extra exploitation as the count value rises. However, \vec{r}_{d1} and \vec{r}_{d2} are arbitrary vectors within [0, 1].

2. Trapping: In order to characterize the conduct of SH numerically, it is assumed that the finest chase agent has information regarding the spot of the hunt. The remaining chase agents form groups toward the finest chase agent and save the finest results attained so far to restore their spots according to the following Equations (27)–(29)

$$\vec{D}_h = \left| \vec{B} \cdot \vec{P}_h(x) - P(x) \right| \quad (27)$$

$$\vec{P}_k = \vec{P}_h - \vec{E} \cdot \vec{D}_h \quad (28)$$

$$\vec{C}_h = \vec{P}_k + \vec{P}_{k+1} + \dots + \vec{P}_{k+N} \quad (29)$$

\vec{P}_h describes the spot of initial finest SH, and \vec{P}_k describes the spot of further SH. At this time, N designates the figure of SH, which is figured as follows:

$$N = \text{count}_{\text{nos}}(\vec{P}_h, \vec{P}_{h+1}, \vec{P}_{h+2}, \dots, (\vec{P}_h + \vec{M})) \quad (30)$$

\vec{M} is the arbitrary vector in [0.5, 1], the numbers outline the figure of the results and the totality of all the contender results, afterward adding \vec{M} , which is far from comparable to the finest ideal result in the specified hunt space, and \vec{C}_h , which is an assembly of N figure of ideal results.

3. Encroaching hunt (exploitation): To numerically model for invading the hunt, the \vec{h} value is lessened. The disparity in \vec{E} is also reduced from 5 to 0 in due course of the count. $|E| < 1$ forces the assembly of SH to attack on the way to the hunt. The numerical design for invading the hunt is

$$\vec{P}(x+1) = \frac{c_h}{N} \quad (31)$$

$\vec{P}(x+1)$ stores the finest result and revises the spot of further chase agents as per the spot of the finest chase agent.

4. Hunt for target (exploration): SH mostly chase the hunt, as per the spot of the assembly of the SH that exist in \vec{C}_h . They shift apart from one another to chase and to combat for the hunt. Then, they utilize \vec{E} with arbitrary values >1 or <-1 to compel the chase agents to shift far away from the hunt. This mechanism permits the SHO algorithm to hunt in a wide-reaching manner. The SHO's flowchart is provided in Figure 4.

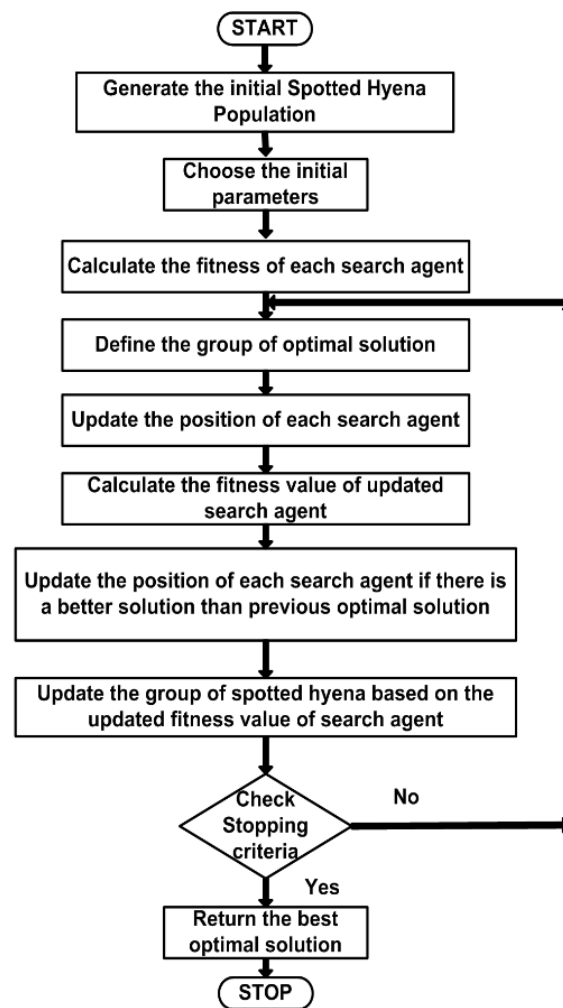


Figure 4. Flowchart of the SHO algorithm.

5. Methodology

A three-area system with a capacity ratio of 2:3:4 is considered for investigation. The investigated system comprises of thermal, bio-diesel, and wave power plant in area-1; thermal and geothermal power plant in area-2; and thermal, split-shaft gas turbine, and solar photovoltaic in area-3. System is also incorporated with an energy storage device. Investigations are carried out considering PDN(FOID) controller whose parameters are obtained by the SHO method with ISE as the performance index. The optimization technique is coded in MATLAB R2022a software, and the investigated system is modeled in Simulink with the FOMCON toolbox.

Studies are carried out for: (1) selection of best controller; (2) selection of appropriate performance index; (3) selection of best optimization method; (4) influence of wave power plant, PV, individually and both together; (5) influence of C^{ES} with or without duple compensation; (6) sensitivity assessment.

6. Outcomes and Valuation

6.1. Evaluation of Dynamic Outcome for the Choice of Superlative Controller

The scheme under evaluation embraces thermal including bio-diesel in area-1, GPP along with thermal in area-2, and Ss (GT) along with thermal in area-3 (Scheme-1). This scheme is familiarized with I/PI/PIDN/FOPID/PDN(FOID) controllers on a specific base. Evaluation is accomplished considering a 1% disturbance of the step content in area-1. The finest obtainable values of individual controller gains and related parameters are

attained by employing SHO by means of Pi_{ISE} . The scheme is initially familiarized through a I controller to attain its gain values and also the parameters of GPP using SHO. The governor and turbine time constants obtained are 0.1 s, respectively. These values of G_{GPP} and T_{GPP} are kept the same for the remainder of the work. Subsequently, PI, PIDN, and FOPID in addition to PDN(FOID) controllers are cast off independently. The finest conceivable values are assembled in Table 1, and dynamic outcomes are associated, as revealed in Figure 5. Significant interpretation of each outcome articulates around the fineness of the PDN(FOID) overtop additional controllers concerning the diminished stage of peak_overshoot (Pk_O), extent-of-oscillations, and peak_undershoot (Pk_U), besides the duration of settling (S_Time). Thus, it is revealed that the SHO-optimized PDN(FOID) controller outperforms other controllers in terms of lessened Pk_O ($\Delta f_1 = 0.0007$ Hz, $\Delta f_2 = 0$ Hz, $\Delta Ptie_{1-2} = 0$ Hz, and $\Delta Ptie_{1-3} = 0$ Hz), Pk_U ($\Delta f_1 = 0.0112$ Hz, $\Delta f_2 = 0.0038$ Hz, $\Delta Ptie_{1-2} = 0.0039$ Hz, and $\Delta Ptie_{1-3} = 0.0039$ Hz), and S_Time ($\Delta f_1 = 25.81$ s, $\Delta f_2 = 35.31$ s, $\Delta Ptie_{1-2} = 21.71$ s, and $\Delta Ptie_{1-3} = 21.04$ s). In Table 2, the matching outcomes of Pk_O, Pk_U, and S_Time values are recorded, which imitates the improved conduct of the PDN(FOID) overtop remainder of the subordinate controllers.

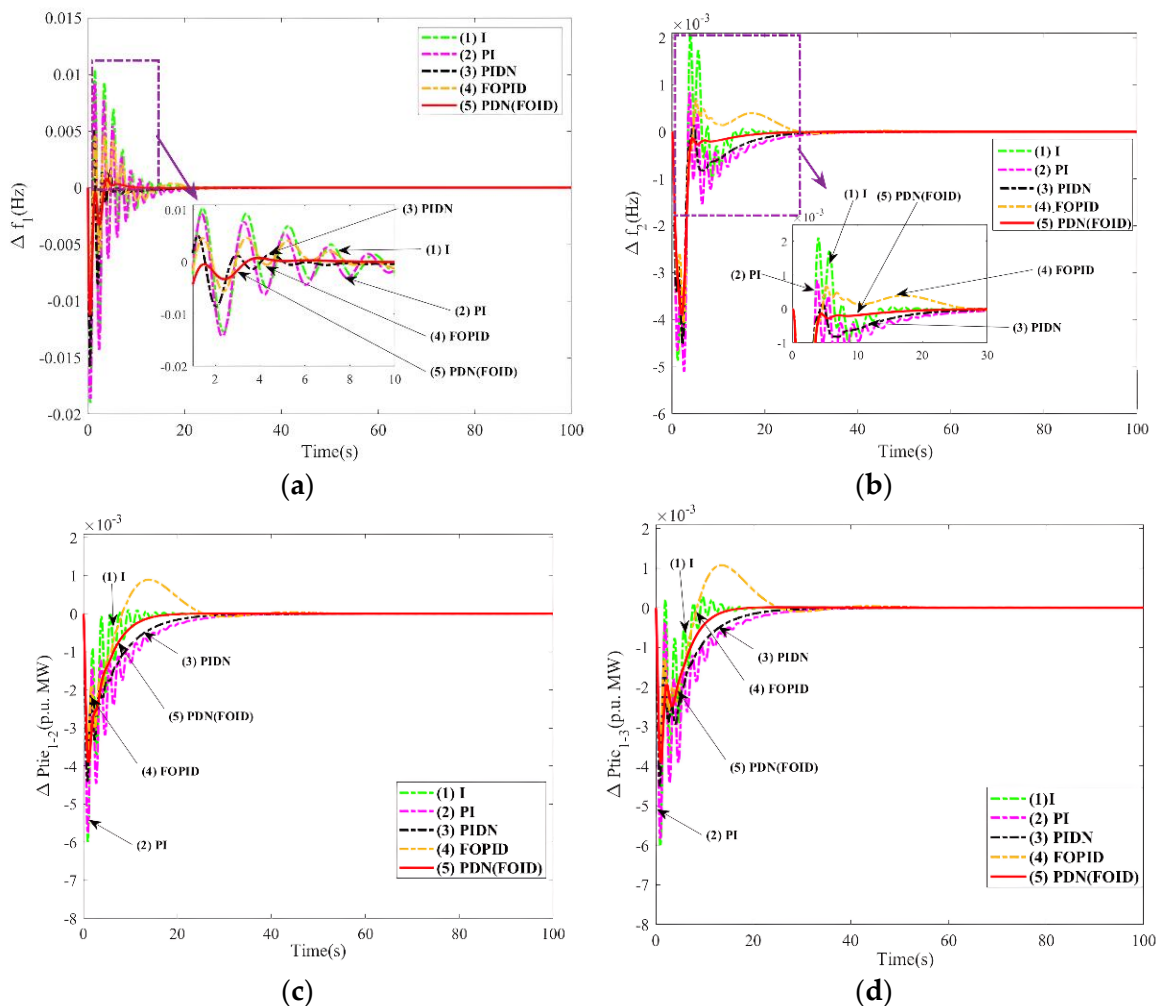


Figure 5. Evaluation of outcomes of subordinate controllers for scheme-1 for 1% step load disorder contrast time: (a) Anomaly of frequency of area-1, (b) Anomaly of frequency of area-2, (c) Anomaly of Tie-line power interlinking area-1 and area-2, (d) Anomaly of Tie-line power interlinking area-1 and area-3.

Table 1. Finest values of gains and related parameters of subordinate controllers for scheme-1.

Name of Controllers	Corresponding Gains and Correlated Parameters	Area-1	Area-2	Area-3
I	K_{Ii}^*	0.9885	0.9897	0.9876
PI	K_{Pi}^*	0.3565	0.5533	0.5538
	K_{Ii}^*	0.4745	0.6497	0.7584
PIDN	K_{Pi}^*	0.6975	0.9728	0.9739
	K_{Ii}^*	0.5982	0.9836	0.9878
	K_{Di}^*	0.6315	0.3140	0.3041
	N_i^*	10.77	11.41	11.25
FOPID	K_{FPI}^*	0.0094	0.0095	0.0096
	K_{FII}^*	0.3765	0.8354	0.9379
	λ_i	1.4352	1.1876	1.1587
	K_{FDi}^*	0.4549	0.6357	0.5366
	μ_i^*	1.0477	0.0768	0.1585
PDN(FOID)	K_{Pi}^*	0.8686	0.5188	0.6875
	K_{Di}^*	0.5796	0.7362	0.9421
	N_i^*	55.58	68.83	79.77
	K_{FII}^*	0.9976	0.9041	0.7454
	λ_i^*	1.0099	0.9454	0.9710
	K_{FDi}^*	0.8508	0.8261	0.8554
	μ_i^*	0.7853	0.2804	0.7216

* Signify the optimum values.

Table 2. Peak anomaly and duration of settling for outcomes in Figure 5 in the case of system-1 employing SHO-optimized I/PI/PIDN/FOPID/PDN(FOID) controllers.

Responses	Name of Controllers	Pk_O	Pk_U	S_Time (in Seconds)
Δf_1 (Figure 5a)	I	0.0103	0.0191	39.42
	PI	0.0092	0.0186	35.53
	PIDN	0.0051	0.0156	31.42
	FOPID	0.0045	0.0113	27.84
	PDN(FOID)	0.0007	0.0112	25.81
Δf_2 (Figure 5b)	I	0.0021	0.0048	43.52
	PI	0.0008	0.0051	42.23
	PIDN	0.0001	0.0045	39.63
	FOPID	0.0006	0.0041	39.97
	PDN(FOID)	0	0.0038	35.31
ΔP_{tie1-2} (Figure 5c)	I	0.0001	0.0059	39.45
	PI	0	0.0057	39.41
	PIDN	0	0.0044	34.24
	FOPID	0.0008	0.0041	33.87
	PDN(FOID)	0	0.0039	21.71
ΔP_{tie1-3} (Figure 5d)	I	0.0002	0.0062	42.23
	PI	0	0.0058	34.88
	PIDN	0	0.0044	34.24
	FOPID	0.0011	0.0041	37.02
	PDN(FOID)	0	0.0039	21.04

6.2. Nomination of Performance Index

The excellent outcome of the performance index (P_i) among the integral squared error (P_{iISE}), integral time squared error (P_{iITSE}), integral absolute error (P_{iIAE}), and integral time absolute error (P_{iITAE}) are procured by assisting system-1 with each of the P_i on individual terms using the PDN(FOID) controller. The premium standards of PDN(FOID) controller

gains and related parameters are attained using the SHO algorithm. The expressions for Pi_{ITSE} , Pi_{IAE} , and Pi_{ITAE} are given by (32)–(34), respectively, and for Pi_{ISE} , it is given by (5)

$$Pi_{ITSE} = \int_0^T \{(\Delta f_1)^2 + (\Delta f_2)^2 + (\Delta f_3)^2 + (\Delta P_{tie_{1-2}})^2 + (\Delta P_{tie_{2-3}})^2 + (\Delta P_{tie_{1-3}})^2\} t dt \quad (32)$$

$$Pi_{IAE} = \int_0^T \{|\Delta f_1| + |\Delta f_2| + |\Delta f_3| + |\Delta P_{tie_{1-2}}| + |\Delta P_{tie_{2-3}}| + |\Delta P_{tie_{1-3}}|\} dt \quad (33)$$

$$Pi_{ITAE} = \int_0^T \{|\Delta f_1| + |\Delta f_2| + |\Delta f_3| + |\Delta P_{tie_{1-2}}| + |\Delta P_{tie_{2-3}}| + |\Delta P_{tie_{1-3}}|\} t dt \quad (34)$$

With the help of illustrious values accomplished for PDN(FOID) controller’s gains and correlated parameters in each case, the dynamic responses are contrasted in Figure 6a–c, and the corresponding Pk_O, Pk_U, and S_Time values are marked down in Table 3. A critical view of the responses says that responses considering Pi_{ISE} as Pi have a better performance compared to others with respect to lessened Pk_O, Pk_U, S_Time, and oscillations. Thus, it is revealed that the SHO-optimized PDN(FOID) controller using ISE as a performance index outperforms other Pi in terms of lessened Pk_O ($\Delta f_1 = 0.0007$ Hz, $\Delta f_2 = 0$ Hz, and $\Delta P_{tie_{1-2}} = 0$ Hz), Pk_U ($\Delta f_1 = 0.0112$ Hz, $\Delta f_2 = 0.0038$ Hz, and $\Delta P_{tie_{1-2}} = 0.0039$ Hz), and S_Time ($\Delta f_1 = 25.81$ s, $\Delta f_2 = 35.31$ s, and $\Delta P_{tie_{1-2}} = 21.71$ s). Further, the values of Pi are $Pi_{ISE} = 0.00021$, $Pi_{ITSE} = 0.00084$, $Pi_{IAE} = 0.1053$, and $Pi_{ITAE} = 0.7233$, which reveals the better performance of the system with Pi_{ISE} . The convergence characteristics for system-1 using different Pi ’s is reflected in Figure 6d. It is observed that convergence characteristics using ISE as Pi converge faster in fewer iterations than other Pi ’s.

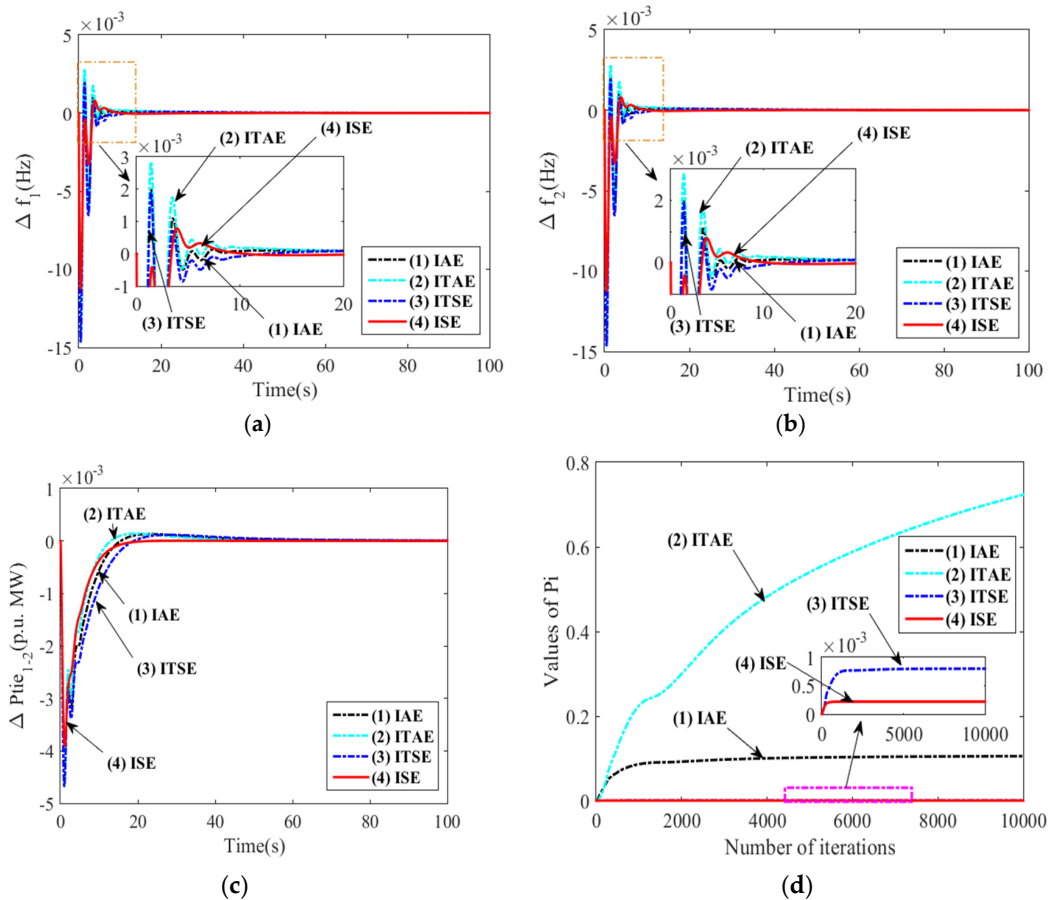


Figure 6. Evaluation for the recommendation of the Pi amongst IAE, ITAE, ITSE, and ISE for employing PDN(FOID) controller in the case of scheme-1 contrast time: (a) Anomaly of frequency of area-1, (b) Anomaly of frequency of area-2, (c) Anomaly of Tie-line power interlinking area-1 and area-2, (d) Convergence curve for the system with different Pi .

Table 3. Peak anomaly and duration of settling for outcomes in Figure 6a–c in the case of scheme-1 employing SHO-optimized PDN(FOID) controller for diverse performance indices.

Responses	Name of Performance Indices	Pk_O	Pk_U	S_Time (in Seconds)
Δf_1 (Figure 6a)	IAE	0.0021	0.0142	29.57
	ITAE	0.0027	0.0145	27.16
	ITSE	0.0019	0.0146	26.65
	ISE	0.0007	0.0112	25.81
Δf_2 (Figure 6b)	IAE	0.0019	0.0144	36.37
	ITAE	0.0028	0.0147	37.72
	ITSE	0.0020	0.0146	36.01
	ISE	0	0.0038	35.31
$\Delta Ptie_{1-2}$ (Figure 6c)	IAE	0.0013	0.0045	44.73
	ITAE	0.0013	0.0046	42.74
	ITSE	0.0001	0.0047	50.24
	ISE	0	0.0039	21.71

6.3. Nomination of Algorithm

For the nomination of the algorithm, system-1 is provided with different algorithms, separately, using PDN(FOID) controllers. The algorithms used here are the firefly algorithm (FA), cuckoo search algorithm (CS) [46], particle swarm optimization (PSO) [47], whale optimization algorithm (WOA), and SHO. The tuned values for FA are $\beta_0 = 0.3$, $\alpha = 0.5$, $\gamma = 0.4$, count of fireflies = 50, and maximum number of generations = 100. For CS, nests count = 50, rate of discovery = 0.5, exponent of levy = 1.5, maximum generation = 100, and count of dimensions = 10. For PSO, the tuned parameters values are $w = 1$, $w_{damp} = 0.99$, $c_1 = 1.4$, $c_2 = 1.98$, population size = 50, and maximum generation number = 100. For WOA, figure of hunt agents = 50, and number of repetitions = 100. For each of the algorithms, the best values for the PDN(FOID) controller are obtained. The values are not provided here. With these values, the responses of different algorithms are contrasted in Figure 7a–c. The corresponding responses of Pk_O, Pk_U, and S_Time values are given in Table 4. In Table 4, it can be seen that Pk_O, Pk_U, and S_Time values obtained by the SHO-optimized PDN(FOID) controller are much better compared to other algorithms. Thus, it is revealed that the SHO-optimized PDN(FOID) controller outperforms other algorithms in terms of lessened Pk_O ($\Delta f_1 = 0.0007$ Hz, $\Delta f_3 = 0$ Hz, and $\Delta Ptie_{1-3} = 0$ Hz), Pk_U ($\Delta f_1 = 0.0112$ Hz, $\Delta f_3 = 0.0052$ Hz, and $\Delta Ptie_{1-3} = 0.0039$ Hz), and S_Time ($\Delta f_1 = 25.81$ s, $\Delta f_3 = 23.53$ s, and $\Delta Ptie_{1-3} = 21.04$ s). Further, the supremacy is judged by the convergence curve provided in Figure 7d, where it is observed that the response with the SHO-optimized PDN(FOID) controller converges faster and has the least value of Pi_{ISE} . Therefore, further analyses are carried out using the SHO algorithm.

Table 4. Peak aberration and duration of settling for outcomes in Figure 7a–c, in the case of system-1 using FA/CS/PSO/WOA/SHO-optimized PDN(FOID) controller on an individual basis.

Responses	Name of Algorithms	Pk_O	Pk_U	S_Time (in Seconds)
Δf_1 (Figure 7a)	FA	0.0026	0.01201	32.95
	CS	0.0029	0.0113	33.79
	PSO	0.0018	0.0013	33.04
	WOA	0.0021	0.0118	29.19
	SHO	0.0007	0.0112	25.81
Δf_3 (Figure 7b)	FA	0.0011	0.0053	36.03
	CS	0.0013	0.0053	30.06
	PSO	0.0008	0.0053	38.04
	WOA	0.0009	0.0055	26.84
	SHO	0	0.0052	23.53

Table 4. Cont.

Responses	Name of Algorithms	Pk_O	Pk_U	S_Time (in Seconds)
$\Delta P_{tie_{1-3}}$ (Figure 7c)	FA	0.0012	0.0041	33.76
	CS	0.0010	0.0041	36.09
	PSO	0.0011	0.0040	37.15
	WOA	0.0006	0.0041	30.23
	SHO	0	0.0039	21.04

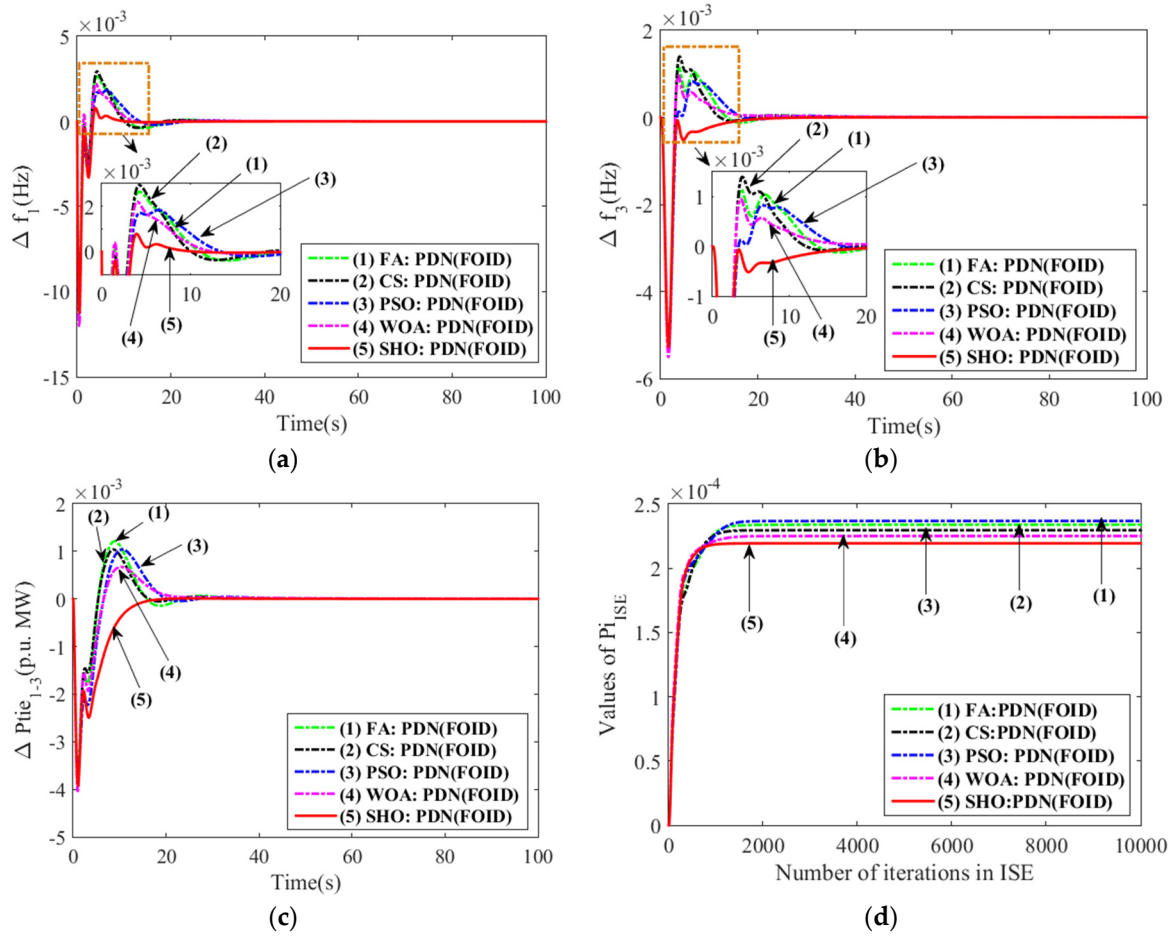


Figure 7. Evaluation for the recommendation of algorithm amid FA/CS/PSO/WOA/SHO techniques for obtaining finest values of PDN(FOID) controller for scheme-1 contrast time: (a) Anomaly of frequency in area-2, (b) Anomaly of Tie-line power interlinking area-1 and area-2, (c) Anomaly of Tie-line power interlinking area-1 and area-3, (d) Convergence curve.

6.4. Evaluation of Influence of the Wave Power Plant on Dynamics of System

In the preceding Section 6.1, it is perceived that the SHO-optimized PDN(FOID) is equipped with admirable pursuance for scheme-1. Now, scheme-1 is integrated with an additional RWS, namely, a wave power plant (WavePPt) in area-1, observed as scheme-2. Forthwith, scheme-2 is integrated with PDN(FOID) as the subservient controller, and the interrelated finest measure of gains in addition to related parameters is accomplished by employing the SHO. The premium values are furnished in Table 5. The assessment is performed for a step change in the WavePPt. With the finest values attained, the evaluation is accomplished for the impact of the WavePPt on the dynamic system by contrasting responses for the system with and without the WavePPt, as in Figure 8. In the outcomes in Figure 8, the vast decline in the values of Pk_U and S_Time is evidently noticeable.

Even Pk_O shows slightly lessened values. With the WavePPt, the values of Δf_2 have shown improvement in Pk_U and S_Time from 0.0038 to 0.00186 Hz (Pk_U) and 35.31 to 30.12 s (in comparison to the system without WavePPt), respectively. Similarly, for Δf_3 , the improvement is 0.0052 to 0.00287 Hz (Pk_U) and 23.53 to 21.96 s; for $\Delta P_{tie_{1-3}}$, the improvement is 0.0039 to 0.00197 Hz and 21.04 to 20.22 s; and for $\Delta P_{tie_{2-3}}$, the improvement is 0.00077 to 0.000381 Hz (Pk_O), 0.00052 to 0.00027 Hz (Pk_U), and 24.65 to 20.09 s. Thus, the presence of the WavePPt improved the dynamics of the scheme.

Table 5. Finest values of gains and related parameters of PDN(FOID) controllers for scheme-2.

Name of Controller	Corresponding Gains and Correlated Parameters	Area-1	Area-2	Area-3
PDN(FOID)	K_{Pi} *	0.9898	0.9687	0.9603
	K_{Di} *	0.9785	0.4252	0.9232
	N_i *	72.24	56.07	78.85
	K_{Fli} *	0.5725	0.5575	0.8418
	λ_i *	1.0484	0.3997	1.0965
	K_{FDi} *	0.9632	0.3326	0.6901
	μ_i *	0.5911	0.7509	0.8949

* Signify optimum values.

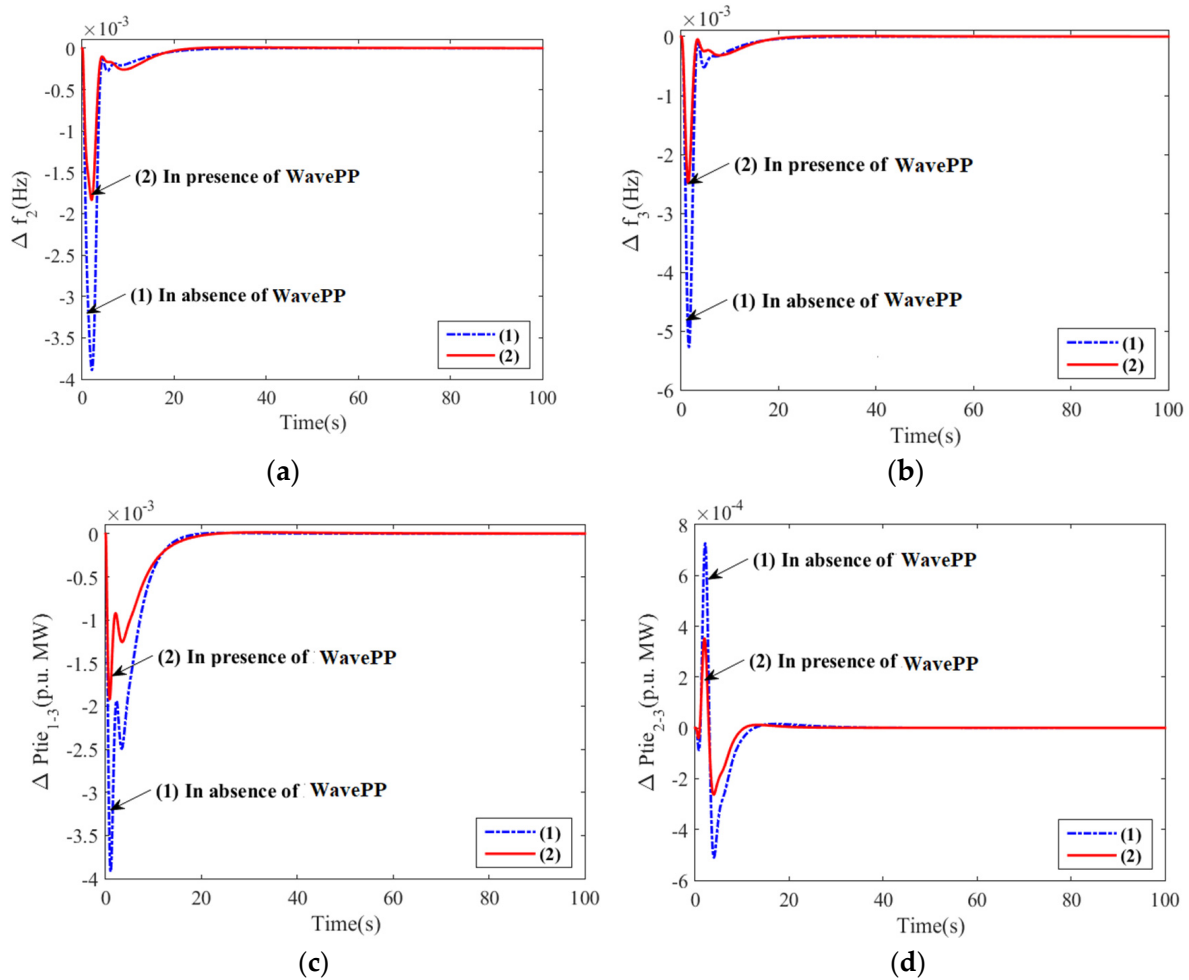


Figure 8. Evaluation of the influence of WavePPt on system changing aspects employing SHO-optimized PDN(FOID) controller in view of 1% step load disturbances for system-2 contrast time: (a) Anomaly of frequency in area-1, (b) Anomaly of frequency in area-3, (c) Anomaly of Tie-line power interlinking area-1 and area-3, (d) Anomaly of Tie-line power interlinking area-2 and area-3.

6.5. Evaluation of Influence of PV on Scheme Dynamics

From the previous analysis in Section 6.1, it can be concluded that the SHO-optimized PDN(FOID) provides with the best performance for system-1 over the I/PI/PIDN/FOPID controllers. Now, system-1 is involved with another RWS, namely, a photovoltaic (PV) unit in area-3, viewed as scheme-3. Then, scheme-3 is included with PDN(FOID) as the subordinate controller in all areas and its finest values of gains and the related parameters are accomplished via the SHO. The finest values are shown in Table 6. Employing the finest values, the evaluation is accomplished for the impact of the PV on a dynamic system by contrasting responses for the system with and without the PV unit, as in Figure 9. In the outcomes in Figure 9, the massive diminution in the values of Pk_O, Pk_U, and S_Time is undoubtedly noticeable. With PV, the values of Δf_1 have shown improvement in Pk_O, Pk_U, and S_Time from 0.0007 to 0 Hz (Pk_O), 0.0112 to 0.00109 Hz (Pk_U), and 25.81 to 20.11 s (in comparison to the system without PV). Similarly, for Δf_2 , the improvement is 0.0038 to 0.00278 Hz (Pk_U) and 35.31 to 33.09 s; for Δf_3 , the improvement is 0.0052 to 0.00298 Hz and 23.53 to 22.54 s; and for $\Delta P_{tie_{2-3}}$, the improvement is 0.00077 to 0.00011 Hz (Pk_O), 0.00052 to 0.000181 Hz (Pk_U), and 24.65 to 20.01 s. Thus, the presence of PV has improved the dynamics of the system.

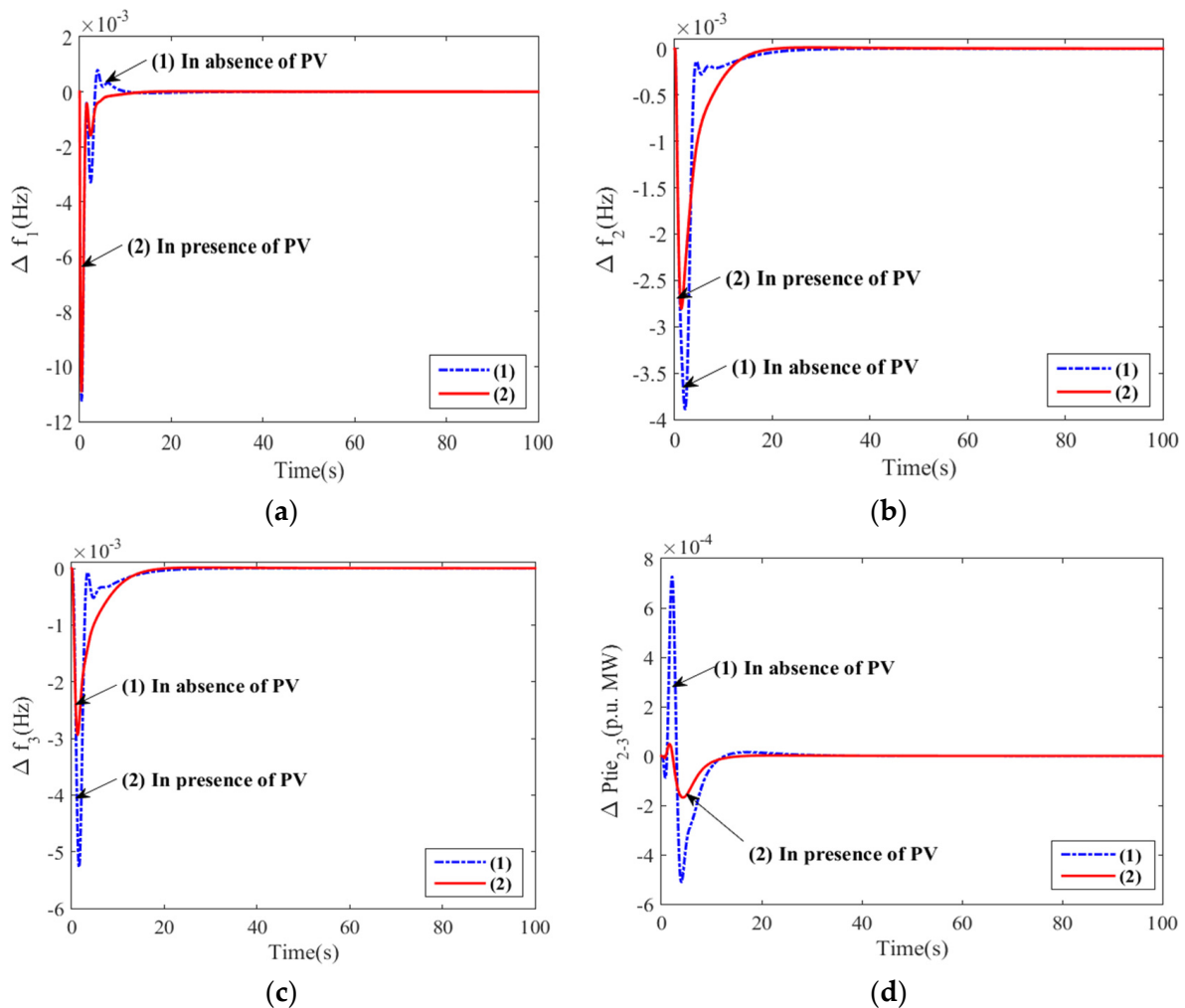


Figure 9. Valuation of influence of PV on system changing aspects employing SHO-optimized PDN(FOID) controller given 1% step load disturbances for system-3 contrast time: (a) Anomaly of frequency in area-1, (b) Anomaly of frequency in area-2, (c) Anomaly of frequency in area-3, (d) Anomaly of Tie-line power interlinking area-2 and area-3.

Table 6. Finest values of gains and related parameters of PDN(FOID) controllers for scheme-3.

Name of Controller	Corresponding Gains and Correlated Parameters	Area-1	Area-2	Area-3
PDN(FOID)	K_{Pi}^*	0.9898	0.6324	0.7416
	K_{Di}^*	0.7992	0.4900	0.4163
	N_i^*	44.42	65.94	44.87
	K_{Fli}^*	0.7752	0.4882	0.6698
	λ_i^*	1.0305	0.6213	0.5595
	K_{FDi}^*	0.8085	0.8341	0.7768
	μ_i^*	0.6545	0.6640	0.7541

* Signify optimum values.

6.6. Assessment of Impact of Both WavePPt and PV on Scheme Dynamics

In the above Sections 6.4 and 6.5, it is observed that RWSs WavePPt and PV, respectively, have a noteworthy impact on the dynamics of the system when assessed individually. Now, system-1 is incorporated with both WavePPt and PV. WavePPt is associated with area-1 and PV in area-3. Thus, this system with both WavePP and PV is considered as system-4. In this case, the SHO-optimized PDN(FOID) controller is also used to analyze the impact of both WavePPt and PV together on the dynamics of the system. The premium standards of gains and related parameters of the PDN(FOID) controller are in Table 7. The dynamic responses for the system with and without both WavePPt and PV are contrasted in Figure 10. Critical assessment in Figure 10 reveals the better performance of the system with both WavePPt and PV with regard to the lessened values of Pk_O, Pk_U, and S_Time. With both WavePPt and PV, the values of Δf_1 showed improvement in Pk_O, Pk_U, and S_Time from 0.0007 to 0.00001 Hz, 0.0112 to 0.0063 Hz, and 25.81 to 22.65 s (in comparison to the system without WavePPt and PV). Similarly, for Δf_2 , the improvement is 0.0038 to 0.00125 Hz (Pk_U) and 35.31 to 27.98 s; for $\Delta Ptie_{1-2}$, the improvement is 0.0039 to 0.00178 Hz and 21.71 to 19.81 s; and for $\Delta Ptie_{1-3}$, the improvement is 0.0039 to 0.00161 Hz and 21.04 to 20.01 s. Thus, the presence of both WavePPt and PV has a noteworthy impact on the system's performance, so further analysis is carried out for both WavePPt and PV.

Table 7. Best values of gains and related parameters of PDN(FOID) controllers for scheme-4 (thermal-bio-diesel-GPP-Ss (GT) system including both WavePPt, PV).

Name of Controller	Corresponding Gains and Correlated Parameters	Area-1	Area-2	Area-3
PDN(FOID)	K_{Pi}^*	0.9899	0.8510	0.6775
	K_{Di}^*	0.5957	0.4620	0.4404
	N_i^*	39.08	50.13	42.96
	K_{Fli}^*	0.4607	0.8522	0.5740
	λ_i^*	1.0916	0.9588	0.7276
	K_{FDi}^*	0.9379	0.8374	0.9869
	μ_i^*	0.9947	0.7315	0.7899

* Signify optimum values.

6.7. Evaluation of the Influence of C^{ES} through/without Duple Compensation on Scheme Changing Aspects

In order to stabilize the system energy storing device, C^{ES} is incorporated into the system. Initially, C^{ES} without duple compensation is integrated into system-4 in all areas. Hence, this is system-5. The best-obtained controller PDN(FOID) from previous sections is used here to assess the impact of the energy-storing device. In this case, the best values of gains and parameters PDN(FOID) obtained using SHO are marked down in Table 8. Next, system-4 is integrated with C^{ES} with duple compensation in all areas. This is considered as system-6. The gains and related parameters of the PDN(FOID) controller for the scheme through C^{ES} involving duple compensation are provided in Table 9. With the values

obtained in Tables 8 and 9, the dynamic responses are plotted and contrasted against the system response without having any forms of CES. This contrast is reflected in Figure 11. In Figure 11, it is observed that any form of C^{ES} has a better impact. However, if the responses for the system with/without C^{ES} with duple compensation are viewed, then they articulate the better performance of the system in existence with C^{ES} with duple compensation in terms of diminished Pk_U and S_Time . With C^{ES} , the values of Δf_2 showed improvement in Pk_U and S_Time from 0.00125 to 0.0008 Hz and 27.98 to 21.82 s (in comparison to the system without energy storage). Similarly, for Δf_3 , the improvement is 0.00125 to 0.00078 Hz and 19.51 to 18.65 s; for $\Delta P_{tie_{1-2}}$, the improvement is 0.00178 to 0.00145 Hz and 19.81 to 17.55 s; for $\Delta P_{tie_{1-3}}$, the improvement is 0.00161 to 0.00143 Hz and 20.01 to 18.65 s. Next, with C^{ES} with duple compensation, the values of Δf_2 showed improvement in Pk_U and S_Time from 0.0008 to 0.0006 Hz and 21.82 to 13.65 s (in comparison to the system with C^{ES}). Similarly, for Δf_3 , the improvement is 0.00078 to 0.00075 Hz and 18.65 to 13.75 s; for $\Delta P_{tie_{1-2}}$, the improvement is 0.00145 to 0.00123 Hz and 18.65 to 16.61 s; for $\Delta P_{tie_{1-3}}$, the improvement is 0.00143 to 0.00132 Hz and 18.65 to 16.58 s. So, C^{ES} with duple compensation will serve better in damping out oscillations and stabilizing the system when there are any fluctuations in demand.

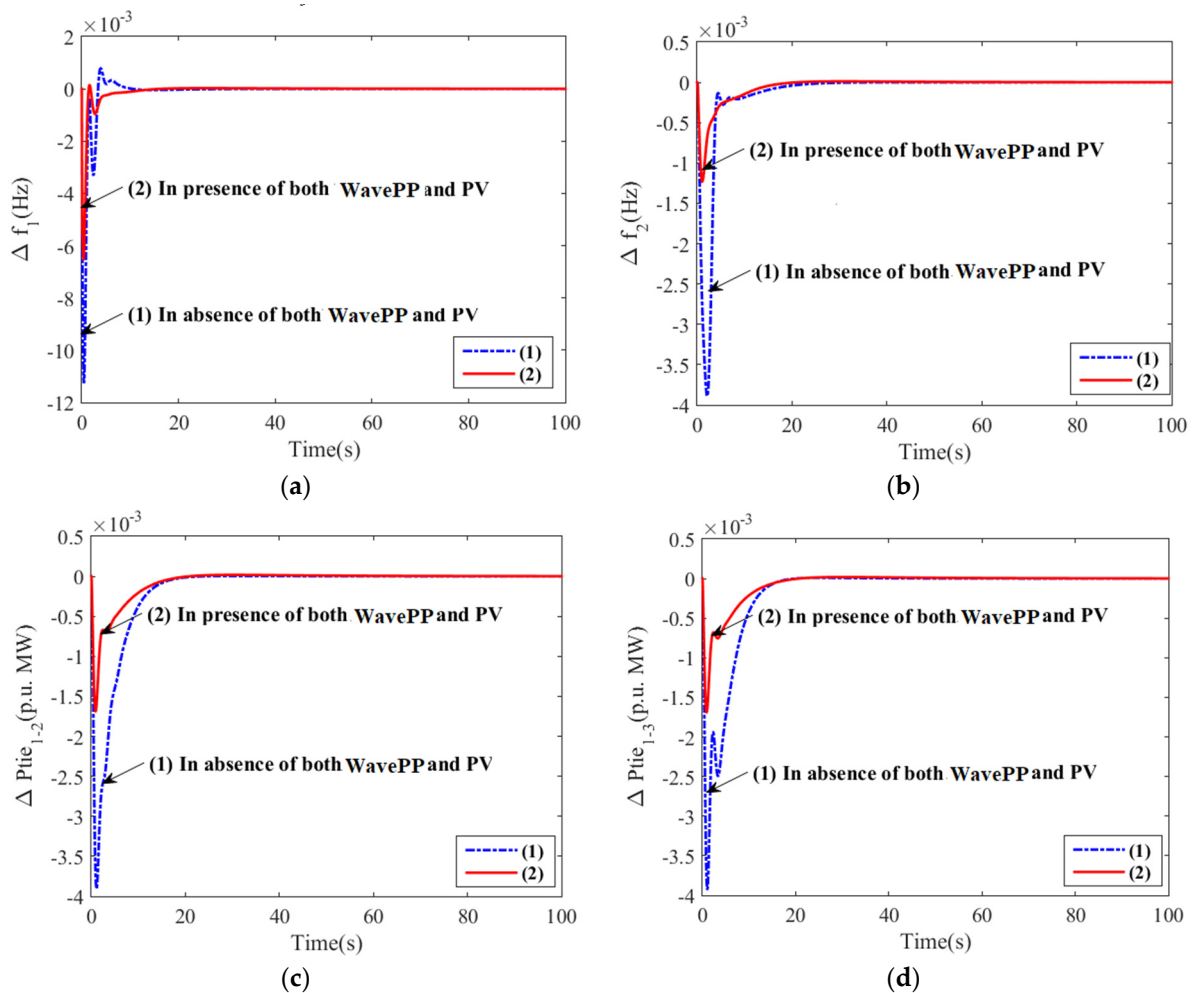


Figure 10. Assessment of the impact of both WavePPt for system-4 contrast time: (a) Anomaly of frequency in area-1, (b) Anomaly of frequency in area-2 vs. time, (c) Anomaly of Tie-line power interlinking area-1 and area-2, (d) Anomaly of Tie-line power interlinking area-1 and area-3.

Table 8. Finest values of gains and related parameters of PDN(FOID) controllers for scheme-5 (thermal-bio-diesel-GPP-Ss (GT) system including WavePPt, PV, and C^{ES} without duple compensation).

Name of Controller	Corresponding Gains and Correlated Parameters	Area-1	Area-2	Area-3
PDN(FOID)	K_{Pi}^*	0.9897	0.9769	0.2093
	K_{Di}^*	0.6681	0.5151	0.8276
	N_i^*	74.90	63.37	93.11
	K_{FHi}^*	0.5953	0.9368	0.5812
	λ_i^*	1.0814	1.2086	0.9863
	K_{FDi}^*	0.8434	0.9893	0.7160
	μ_i^*	0.5678	0.0027	0.6173

* Signify optimum values.

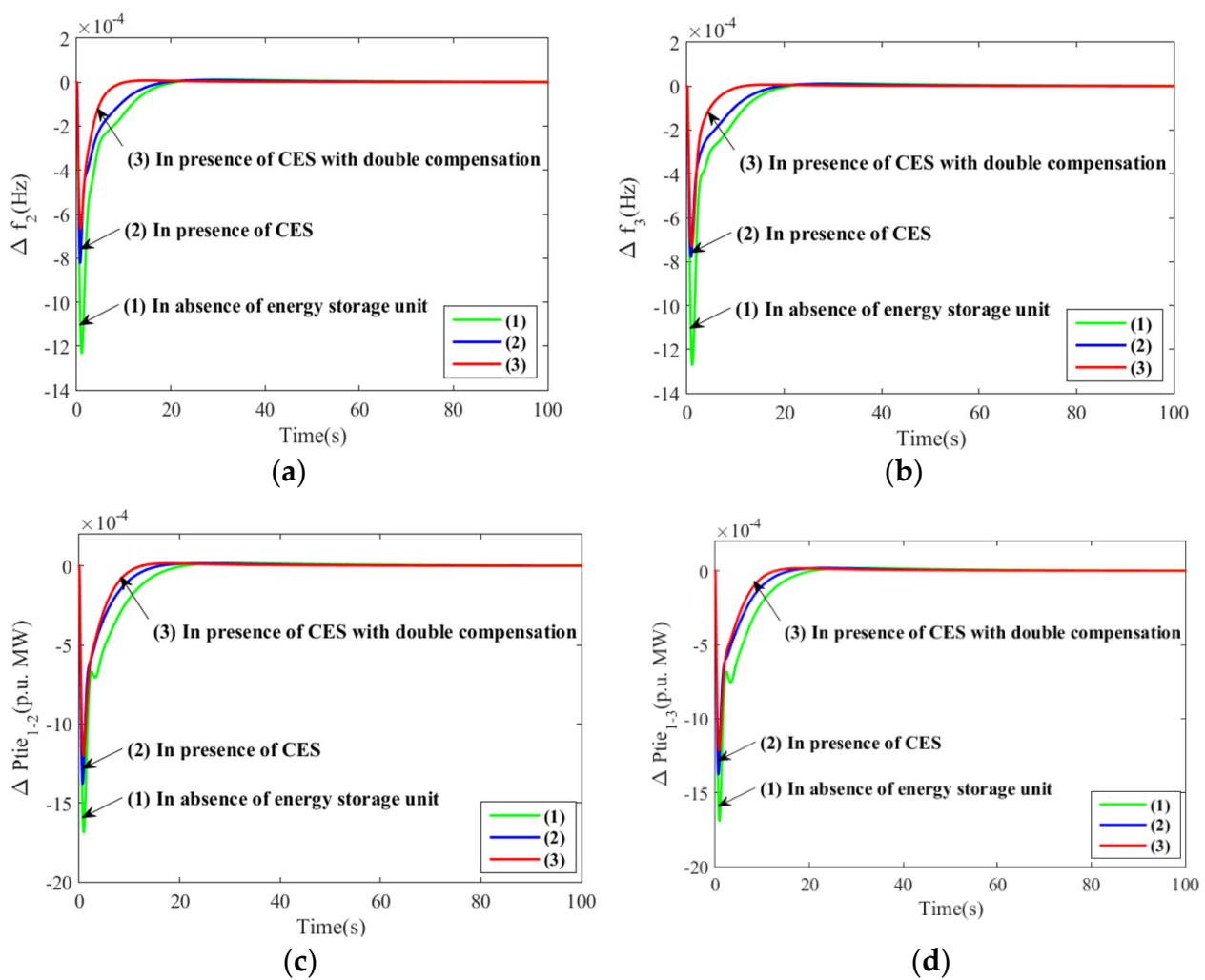


Figure 11. Valuation of influence of C^{ES} with/without duple compensation on scheme dynamics employing SHO-optimized PDN(FOID) controller taking into account 1% step load disturbances for system-5 and system-6 individually contrast time: (a) Anomaly of frequency in area-2, (b) Anomaly of frequency in area-3, (c) Anomaly of Tie-line power interlinking area-1 and area-2, (d) Anomaly of Tie-line power interlinking area-1 and area-3.

Table 9. Finest values of gains and related parameters of PDN(FOID) controllers for scheme-6 (thermal–bio–diesel–GPP–Ss (GT) system including WavePPt, PV, and C^{ES} with duple compensation) (* Signify optimum values).

Name of Controller	Corresponding Gains and Correlated Parameters	Area-1	Area-2	Area-3
PDN(FOID)	K_{Pi} *	0.9899	0.9288	0.1632
	K_{Di} *	0.9785	0.4533	0.4110
	N_i *	44.19	54.55	43.39
	K_{Fli} *	0.8900	0.9529	0.4464
	λ_i *	1.0914	0.0095	0.1938
	K_{FDi} *	0.9632	0.9630	0.7367
	μ_i *	0.7989	0.7919	0.8705

6.8. Sensitivity Determination When Subjected to Random Disturbance

The exploration of sensitivity is executed to perceive the heftiness of SHO-augmented PDN(FOID) controller gains traced at the basic event to comprehensive variance in the structure state of the thermal–bio–diesel–WavePPt in area-1, thermal–GPP in area-2, and thermal–Ss (GT)–PV in area-3 schemes along with C^{ES} with duple compensation. Here, the inspected scheme is stated with a random pattern of disturbance from a basic 1% step load disturbance. The augmented gains of the PDN(FOID) controller reflected in Table 10 are attained by retaining the SHO. The dynamic outcomes for the finest values analogous to the foundation and diverse outcomes are distinguished in Figure 12. In Figure 12a–d, it is indicated that all responses obtained with optimized values for the proposed controller (from Table 9) are stable for random load disturbance. Evaluation affirms that the outcomes are moderately identical, which claims that there are no circumstances for the added retuning of the finest values for modification.

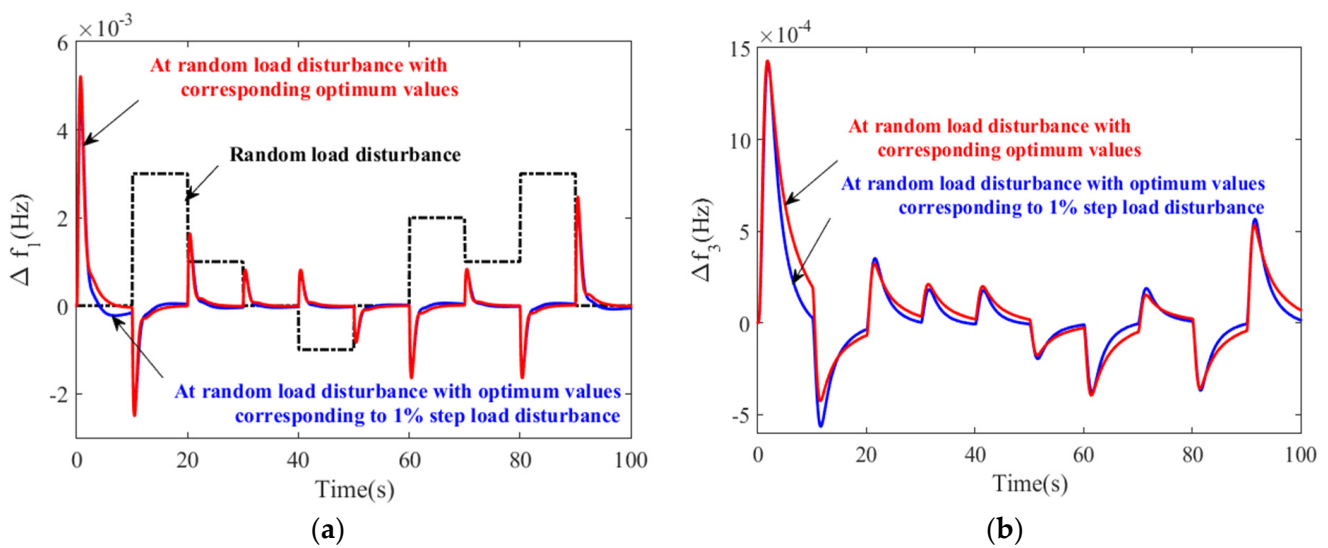


Figure 12. Cont.

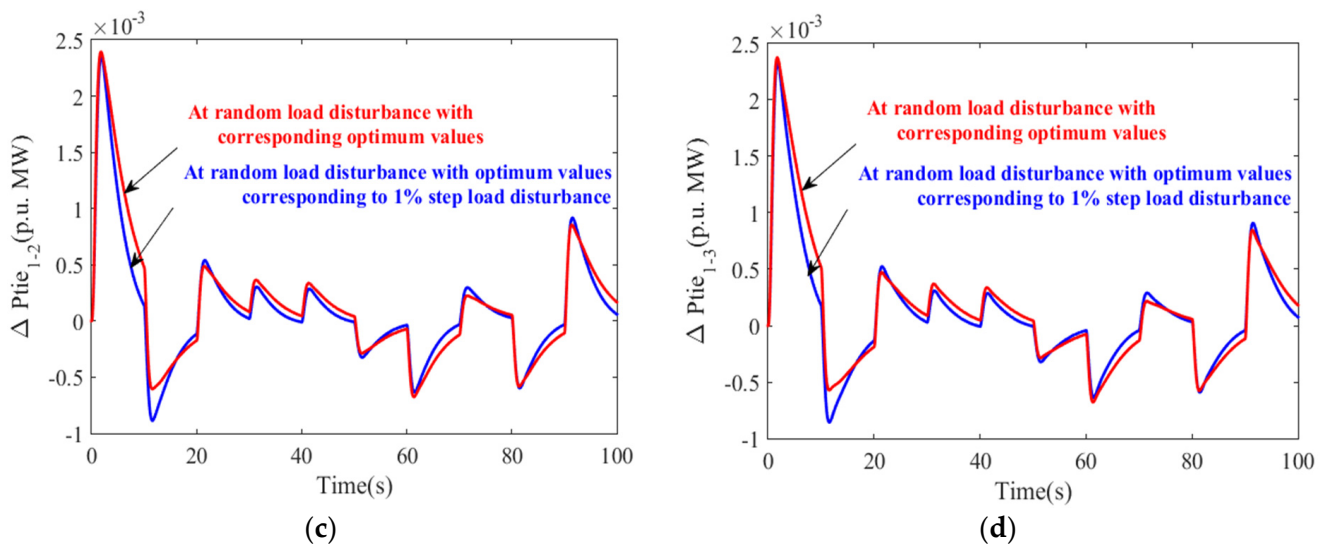


Figure 12. Evaluation of system-6 outcomes employing SHO-optimized PDN(FOID) controller after exposure to random load disturbance contrast time: (a) Anomaly of frequency in area-1, (b) Anomaly of frequency in area-3, (c) Anomaly of Tie-line power interlinking area-1 and area-2, (d) Anomaly of Tie-line power interlinking area-1 and area-3.

Table 10. Finest values of gains and correlated parameters of PDN(FOID) controllers for scheme-6 when conditional to a random pattern of disturbance.

Name of Controller	Corresponding Gains and Correlated Parameters	Area-1	Area-2	Area-3
PDN(FOID)	K_{Pi}^*	0.8095	0.8965	0.2588
	K_{Di}^*	0.8921	0.5145	0.5147
	N_i^*	48.36	62.36	51.36
	K_{Fli}^*	0.8478	0.9147	0.5147
	λ_i^*	1.0549	0.0089	0.2147
	K_{FDi}^*	0.8956	0.8899	0.8144
	μ_i^*	0.6897	0.7514	0.8566

* Signify optimum values.

7. Conclusions

An innovative endeavor was placed to put into effect a two-stage controller through the amalgamation of a proportional-derivative with filter (PDN) (InO) and integral-derivative (FOID) (FrO) in AGC. A lately established biologically influenced meta-heuristic algorithm articulated as the spotted hyena optimizer (SHO) was proficiently employed for attaining gains and additional related parameters of diverse controllers. The superiority of PDN(FOID) was realized over additional classical controllers for the thermal–bio-diesel–geothermal power plant (GPP)–split-shaft gas turbine (Ss (GT)) system. The assessment shows that when the basic system was incorporated with either the wave power plant (WavePPt) or photovoltaic (PV) unit, the system responses improved in terms of lessened peak_overshoot, peak_undershoot, and settling_time using the PDN(FOID) controller. Much better responses were obtained when the system was involved with both the WavePPt and PV. Analysis also revealed the better performance of capacitive energy storage (C^{ES}) with duple compensation over the system with C^{ES} without duple compensation and systems without any form of C^{ES} . The robustness of the PDN(FOID) controller was undertaken by examining the system (having WavePPt, PV, and C^{ES} with duple compensation) when subjected to a random load of disturbance. It demonstrated that the finest values attained, considering PDN(FOID) gains and additional related constraints, were satisfactory and sufficient, and there were not, by any means, alterations under random load.

Author Contributions: Conceptualization, A.S. and P.D.; methodology, N.R.B.; software, T.C.; validation, A.S., P.D. and N.R.B.; formal analysis, N.R.B.; investigation, A.S.; resources, T.C. and B.V.; data curation, T.C.; writing—original draft preparation, A.S.; writing—review and editing, A.S., T.C., B.V. and Ł.K.; visualization, P.D.; supervision, N.R.B.; adaptation of optimization procedure, Ł.K. All authors have read and agreed to the published version of the manuscript.

Funding: Optimization procedure research was partially supported by the Poznan University of Technology, grant number (0212/SBAD/0568).

Institutional Review Board Statement: Not applicable.

Informed Consent Statement: Not applicable.

Data Availability Statement: Not applicable.

Conflicts of Interest: The authors declare no conflict of interest.

Nomenclature

f	Balance point valuation of frequency measured in Hertz (Hz).
*	Best aggregate suggested by exponent.
k	Count of areas suggested.
B_k	Portion of frequency bias of areas engaged.
T_{kj}	Portion of synchronization.
T	Total moment of simulation measured in seconds.
Δf_k	Modification of frequency of areas engaged.
ΔP_{Dk}	Degree of load modification of areas engaged.
H_k	Degree of inertia constant of areas engaged.
D_k	Degree of load modification of areas engaged (p.u. MW)/Modification of frequency of areas engaged (Hz).
R_k	Factor related to governor's speed regulation of area suggested.
β_k	Attributions of frequency outcome of area suggested.
K_{pk}	Gain constant of power system representation.
T_{pk}	Time constant of power system prototypes.
P_{rk}	Considerable rated power of area suggested.
a_{kj}	Considerable rated power of area-k/Considerable rated power of area-j
pf	Area contribution factor.
T_g, T_t, T_r	Time constants of thermal generating parts in seconds (s).
K_r	Reheater's gain.

Appendix A

1. Basic Power System: $f = 60$ Hz; Primary loading = 50%, $K_{pm} = 120$ Hz/p.u. MW, $T_{pm} = 20$ s, $T_m = 0.086$ s, $H_m = 5$ s; $D_m = 0.00833$ p.u. MW/Hz; $\beta_m = 0.425$ p.u. MW/Hz; $R_m = 2.4$ Hz/p.u. MW
2. Thermal: $T_{rm} = 10$ s, $K_{rm} = 5$, $T_{tm} = 0.3$ s, $T_{gm} = 0.08$ s;
3. Bio-diesel: $K_{vr} = 1$, $T_{vr} = 0.05$ s, $K_{ce} = 1$, $T_{ce} = 0.5$ s;
4. Ss(GT): $L_{max} = 1$, $T_3 = 3$ s, $T_1 = T_2 = 1.5$ s, $K_T = 1$, $FOV_{max} = 1$, $FOV_{min} = -0.02$, $D_{tur} = 0$ p.u.;
5. CES: $K_{CES} = 0.3$, $T_{CES} = 0.0352$ s;
6. CES with duple compensation: K_{CES} (duple compensation) = 0.3, T_{CES} (duple compensation) = 0.046 s, $T_1 = 0.280$, $T_2 = 0.025$, $T_3 = 0.0411$, $T_4 = 0.39$;
7. PV: $A = 900$, $B = -18$, $C = 100$, $D = 50$.

References

1. Elgerd, O.I. *Electric Energy Systems Theory: An Introduction*; McGraw-Hill: New Delhi, India, 2007.
2. Kundur, P. *Power System Stability and Control*; McGraw-Hill: New Delhi, India, 1993.
3. Ibraheem Kumar, P.; Kothari, D.P. Recent philosophies of automatic generation control strategies in power systems. *IEEE Trans. Power Syst.* **2005**, *20*, 346–357. [[CrossRef](#)]

4. Das, D.; Aditya, S.K.; Kothari, D.P. Dynamics of diesel and wind turbine generators on an isolated power system. *Electr. Power Energy Syst.* **1999**, *21*, 183–189. [[CrossRef](#)]
5. Das, D.C.; Roy, A.K.; Sinha, N. GA based frequency controller for solar thermal–diesel–wind hybrid energy generation/energy storage system. *Int. J. Electr. Power Energy Syst.* **2012**, *43*, 262–279. [[CrossRef](#)]
6. Ismayil, C.; Sreerama, K.R.; Sindhu, T.K. Automatic generation control of single area thermal power system with fractional order PID (PIAD μ) controllers. In Proceedings of the 3rd International Conference on Advances in Control and Optimization of Dynamical Systems, Kanpur, India, 13–15 March 2014; pp. 552–557.
7. Elgerd, O.I.; Fosha, C.E. Optimum Megawatt-Frequency Control of Multiarea Electric Energy Systems. *IEEE Trans. Power Appar. Syst.* **1970**, *89*, 556–563. [[CrossRef](#)]
8. Bhatt, P.; Roy, R.; Ghoshal, S.P. GA/particle swarm intelligence based optimization of two specific varieties of controller devices applied to two-area multi-units automatic generation control. *Int. J. Electr. Power Energy Syst.* **2010**, *32*, 299–310. [[CrossRef](#)]
9. Nanda, J.; Saikia, L.C. Comparison of performances of several types of classical controller in automatic generation control for an interconnected multi-area thermal system. In Proceedings of the Power Engineering Conference, 2008. AUPEC '08. Australasian Universities, Sydney, Australia, 14–17 December 2008.
10. Nanda, J.; Mishra, S.; Saikia, L.C. Maiden application of bacterial foraging based optimization technique in multi area automatic generation control. *IEEE Trans. Power Syst.* **2009**, *24*, 602–609. [[CrossRef](#)]
11. Golpira, H.; Bevrani, H.; Golpira, H. Application of GA optimization for automatic generation control design in an interconnected power system. *Energy Convers. Manag.* **2011**, *52*, 2247–2255. [[CrossRef](#)]
12. Dhamanda, A.; Dutt, A.; Bhardwaj, A.K. Automatic Generation Control in Four Area Interconnected Power System of Thermal Generating Unit through Evolutionary Technique. *Int. J. Electr. Eng. Inform.* **2015**, *7*, 569–583.
13. Saikia, L.C.; Nanda, J.; Mishra, S. Performance comparison of several classical controllers in AGC for multi-area interconnected thermal system. *Int. J. Electr. Power Energy Syst.* **2011**, *33*, 394–401. [[CrossRef](#)]
14. Nanda, J.; Mangla, A.; Suri, S. Some new findings on automatic generation control of an interconnected hydrothermal system with conventional controllers. *IEEE Trans. Energy Convers.* **2006**, *21*, 187–194. [[CrossRef](#)]
15. Saikia, L.C.; Chowdhury, A.; Shakya, N.; Shukla, S.; Soni, P.K. AGC of a multi area thermal system using firefly optimized IDF controller. In Proceedings of the 2013 Annual IEEE India Conference (INDICON), Mumbai, India, 13–15 December 2013.
16. Pradhan, P.C.; Sahu, R.K.; Panda, S. Firefly algorithm optimized fuzzy PID controller for AGC of multi-area multi-source power systems with UPFC and SMES. *Eng. Sci. Technol. Int. J.* **2016**, *19*, 338–354. [[CrossRef](#)]
17. Saha, A.; Saikia, L.C. Renewable energy source-based multiarea AGC system with integration of EV utilizing cascade controller considering time delay. *Int. Trans. Electr. Energy Syst.* **2019**, *29*, e2646. [[CrossRef](#)]
18. Arya, Y. AGC of PV-thermal and hydro-thermal energy systems using CES and a new multistage FPIDF-(1+PI) controller. *Renew. Energy* **2019**, *134*, 796–806. [[CrossRef](#)]
19. Tasnin, W.; Saikia, L.C. Performance comparison of several energy storage devices in deregulated AGC of a multi-area system incorporating geothermal power plant. *IET Renew. Power Gener.* **2018**, *12*, 761–772.
20. Barik, A.K.; Das, D.C. Expedient frequency control of solar photobiotic/biogas/biodiesel generator based isolated renewable microgrid using Grasshopper Optimisation Algorithm. *IET Renew. Power Gener.* **2018**, *12*, 1659–1667.
21. Hasanien, M.H. Whale optimisation algorithm for automatic generation control of interconnected modern power systems including renewable energy sources. *IET Gener. Transm. Distrib.* **2018**, *12*, 607–614.
22. Dhundhara, S.; Verma, Y.P. Capacitive energy storage with optimized controller for frequency regulation in realistic multisource deregulated power system. *Energy* **2018**, *147*, 1108–1128.
23. Pathak, N.; Verma, A.; Bhatti, T.S.; Nasiruddin, I. Modeling of HVDC tie-links and their utilization in AGC/LFC operations of multi-area power systems. *IEEE Trans. Ind. Electron.* **2019**, *66*, 2185–2197. [[CrossRef](#)]
24. Kumari, N.; Malik, N.; Jha, A.N.; Mallesham, G. Design of PI Controller for Automatic Generation Control of Multi Area Interconnected Power System using Bacterial Foraging Optimization. *Int. J. Eng. Technol.* **2016**, *8*, 2779–2786. [[CrossRef](#)]
25. Jagatheesan, K.; Anand, B.; Samanta, S.; Dey, N.; Ashour, A.S.; Balas, V.E. Design of a proportional-integral-derivative controller for an automatic generation control of multi-area power thermal systems using firefly algorithm. *IEEE/CAA J. Autom. Sin.* **2019**, *6*, 503–515.
26. Dash, P.; Saikia, L.C.; Sinha, N. Comparison of performances of several FACTS devices using Cuckoo search algorithm optimized 2DOF controllers in multi-area AGC. *Electr. Power Energy Syst.* **2015**, *65*, 316–324. [[CrossRef](#)]
27. Rahman, A.; Saikia, L.C.; Sinha, N. AGC of dish-stirling solar thermal integrated thermal system with biogeography based optimised three degree of freedom PID controller. *IET Renew. Power Gener.* **2016**, *10*, 1161–1170. [[CrossRef](#)]
28. Reddy, P.J.; Kumar, T.A. AGC of three-area hydro-thermal system in deregulated environment using FOPI and IPFC. In Proceedings of the 2017 International Conference on Energy, Communication, Data Analytics and Soft Computing (ICECDS), Chennai, Indian, 1–2 August 2017; pp. 2815–2821. [[CrossRef](#)]
29. Pan, I.; Das, S. Fractional order AGC for distributed energy resources using robust optimization. *IEEE Trans. Smart Grid* **2016**, *7*, 2175–2186. [[CrossRef](#)]
30. Dash, P.; Saikia, L.C.; Sinha, N. Automatic generation control of multi area thermal system using Bat algorithm optimized PD–PID cascade controller. *Int. J. Electr. Power Energy Syst.* **2015**, *68*, 364–372. [[CrossRef](#)]

31. Saha, A.; Saikia, L.C. Utilisation of ultra-capacitor in load frequency control under restructured STPP-thermal power systems using WOA optimised PIDN-FOPD controller. *IET Gener. Transm. Distrib.* **2017**, *11*, 3318–3331. [[CrossRef](#)]
32. Sahu, R.K.; Panda, S.; Rout, U.K.; Sahoo, D.K. Teaching learning based optimization algorithm for automatic generation control of power system using 2-DOF PID controller. *Int. J. Elect. Power Energy Syst.* **2016**, *77*, 287–301. [[CrossRef](#)]
33. Haroun, A.H.G.; Li, Y.-Y. A novel optimized hybrid fuzzy logic intelligent PID controller for an interconnected multi-area power system with physical constraints and boiler dynamics. *ISA Trans.* **2017**, *71*, 364–379. [[CrossRef](#)]
34. Padhan, S.; Sahu, R.K.; Panda, S. Application of firefly algorithm for load frequency control of multi-area interconnected power system. *Electr. Power Compon. Syst.* **2014**, *42*, 1419–1430. [[CrossRef](#)]
35. Sharma, Y.; Saikia, L.C. Automatic generation control of a multi-area ST—thermal power system using Grey Wolf Optimizer algorithm based classical controllers. *Electr. Power Energy Syst.* **2015**, *73*, 853–862. [[CrossRef](#)]
36. Kumar, N.; Kumar, V.; Tyagi, B. Multi area AGC scheme using imperialist competition algorithm in restructured power system. *Appl. Soft Comput.* **2016**, *48*, 160–168. [[CrossRef](#)]
37. Dash, P.; Saikia, L.C.; Sinha, N. Flower pollination algorithm optimized PI-PD cascade controller in automatic generation control of a multi-area power system. *Int. J. Electr. Power Energy Syst.* **2016**, *82*, 19–28. [[CrossRef](#)]
38. Khan, M.H.; Ulasayar, A.; Khattak, A.; Zad, H.S.; Alsharef, M.; Alahmadi, A.A.; Ullah, N. Optimal Sizing and Allocation of Distributed Generation in the Radial Power Distribution System Using Honey Badger Algorithm. *Energies* **2022**, *15*, 5891. [[CrossRef](#)]
39. Sun, S.; Zhang, Q.; Sun, J.; Cai, W.; Zhou, Z.; Yang, Z.; Wang, Z. Lead–Acid Battery SOC Prediction Using Improved AdaBoost Algorithm. *Energies* **2022**, *15*, 5842. [[CrossRef](#)]
40. Zhu, L.; He, J.; He, L.; Huang, W.; Wang, Y.; Liu, Z. Optimal Operation Strategy of PV-Charging-Hydrogenation Composite Energy Station Considering Demand Response. *Energies* **2022**, *15*, 5915. [[CrossRef](#)]
41. Dhiman, G.; Kumar, V. Spotted hyena optimizer: A novel bio-inspired based metaheuristic technique for engineering applications. *Adv. Eng. Softw.* **2017**, *114*, 48–70. [[CrossRef](#)]
42. Chiranjeevi, T.; Biswas, R.K. Discrete-Time Fractional Optimal Control. *Mathematics* **2017**, *5*, 25. [[CrossRef](#)]
43. Chiranjeevi, T.; Biswas, R.K. Closed-Form Solution of Optimal Control Problem of a Fractional Order System. *J. King Saud Univ. –Sci.* **2019**, *31*, 1042–1047. [[CrossRef](#)]
44. Chiranjeevi, T.; Biswas, R.K.; Devarapalli, R.; Babu, N.R.; Marquez, P.G. On optimal control problem subject to fractional order discrete time singular systems. *Arch. Control. Sci.* **2021**, *31*, 849–863.
45. Oustaloup, A.; Mathieu, B.; Lanusse, P. The CRONE Control of Resonant Plants: Application to a Flexible Transmission. *Eur. J. Control.* **1995**, *1*, 113–121. [[CrossRef](#)]
46. Knypiński, Ł.; Kuroczycki, S.; Márquez, F.P.G. Minimization of Torque Ripple in the Brushless DC Motor Using Constrained Cuckoo Search Algorithm. *Electronics* **2021**, *10*, 2299.
47. Devarapalli, R.; Kumar Sinh, N.; Bathinavenkateswara, R.; Knypiński, Ł.; Jaya Naga, N.; Marquez, F.P.G. Allocation of real power generation based on computing over all generation cost: An approach of Salp Swarm Algorithm. *Arch. Electr. Eng.* **2021**, *70*, 337–349. [[CrossRef](#)]